National Aeronautics and Space Administration

IUE OBSERVING PROGRAM

FINAL TECHNICAL REPORT FOR NAG 5-1140

Submitted to:

Dr. Y. Kondo
Code 684
Laboratory for Astronomy & Solar Physics
Space and Earth Sciences Directorate
Goddard Space Flight Center
Greenbelt, MD 20771

Submitted by:

The Trustees of Columbia University
in the City of New York
Box 20, Low Memorial Library
New York, New York 10027

Prepared by:

Columbia Astrophysics Laboratory
Departments of Astronomy and Physics
Columbia University
538 West 120th Street
New York, New York 10027

Title of Research:

Search for Correlated UV and X-ray Absorption of NGC3516

Principal Investigator:

Christopher Martin
Associate Professor of Physics

Co-Investigators:

Jules P. Halpern
Associate Professor of Physics

Michiel Kolman
Graduate Research Assistant

Period Covered by Report:

15 June 1989 – 31 December 1990

TABLE OF CONTENTS

1. Introduction 1

2. Observations 2

3. Results 3

   3.1. Short-term UV Variability 3

   3.2. Emission Lines 4

   3.3. Galactic Absorption Lines 5

   3.4. The C IV, N V, and Si IV Absorption Features 5

   3.5. Lower Limit on the Carbon Column Density 7

   3.6. Estimate of the Distance from the Absorber to the Continuum Source . . . 8

   3.7. Variability in the Continuum and Absorption 8

4. Discussion 10

   4.1. A Comparison with BAL QSOs 10

   4.2. The X-ray – UV Connection 13

5. Conclusions 16

6. Continuing and Future Work 17

Tables 18

References 21

Figure Captions 22

Figures 23

Appendix: Papers Published Under NASA Grant NAG 5-1140 27

SEARCH FOR CORRELATED UV AND X-RAY ABSORPTION IN NGC 3516

Final Technical Report

1. INTRODUCTION

NGC 3516, a low-luminosity Seyfert galaxy, is one of a small fraction of Seyfert galaxies that exhibit broad absorption in a resonance line. Ulrich and Boisson (1983) first found that the C IV λ1550, N V λ1240, and Si IV λ1440 emission lines all contain broad (EW $\sim$ 9Å) absorption lines blueshifted with respect to the narrow lines. Voit, Shull, and Begelman (1987, hereafter VSB) used archival IUE data to demonstrate variability of the equivalent width, redshift, and line profiles on time scales as short as one week. In one 2 week period, the line profile change had a P Cygni form, possibly indicating radial outflow of the UV absorbing gas. Since the absorption feature is often deeper than either the emission line or the continuum level alone, the absorbing gas must partially cover both the broad-line gas and the central continuum source.

NGC 3516 also undergoes rapid X-ray spectral variations that have been attributed in part to variable photoelectric absorption (Halpern 1982; Reichert et al. 1985). Two models have been proposed to account for this behavior. In the "cold absorbers" model, clouds of moderate temperature and ionization parameter partially cover the X-ray source, with orbital motion producing the variable covering. The absorbers can be identified with the broad emission-line clouds, since the inferred column densities ($\sim 10^{23}\,\mathrm{cm}^{-2}$) and temperatures ($T \sim 10^4$ K) are comparable. An alternative model was proposed by Halpern (1984), invoking warm clouds, whose ionization balance can be strongly influenced by a variable nuclear continuum. When the ionization parameter is high, H and He are completely stripped, and the soft X-rays are unattenuated, while there is significant absorption near 1 keV due to continuum absorption by O^{+6} and O^{+7}. Reichert, Mushotzky, and Holt (1986) proposed that the X-ray and UV absorption have a common origin in the broad

emission-line clouds. VSB argue against this hypothesis, based primarily on the large velocity coverage of the absorption line compared to that predicted in individual broad-line clouds. However, they do not rule out the possibility of common UV and X-ray absorption in gas other than the broad-line clouds.

2. OBSERVATIONS

In order to determine whether the UV and X-ray absorption in NGC 3156 are related, 5 *IUE* observations were obtained in October, 1989, qusai-simultaneously with 4 Ginga observations. All the new *IUE* observations are listed in Table 1. The images were obtained with the large aperture in the low dispersion mode, resulting in a spectral resolution of $\sim$ 5 Å and $\sim$ 8 Å for the SWP and LWP, respectively.

The spectra obtained on October 19 were severely contaminated by increased background radiation due to solar flare activity. These spectra were found to be useless and were excluded from further data analysis. Four SWP and three LWP spectra of optimal quality were taken approximately equally spaced in time and spanning nine days all together. In these spectra, we flagged the data points due to saturation, cosmic ray hits or the presence of reseaux. The coadded spectra are shown in Figure 1, and the the individual good SWP spectra are in Figure 2. Optimal exposure in the C IV λ1550 line was achieved, and showed deep absorption. Only 3 out of the 4 Ginga observations were successful.

These spectra were produced from the line-by-line images with the Gaussian extraction (GEX) routines (Urry & Reichert 1988) at the Goddard Regional Data Analysis Facility. In short, these routines fit a Gaussian at each wavelength along the spatial direction of the image. Subsequently, these fits are required to vary smoothly along the spectral direction. This procedure minimizes the noise from the extraction process while maintaining an accurate flux level. At a distance of 27 Mpc ($z = 0.009$; $H_0 = 100$ km s^{-1} Mpc^{-1} and q_0=0 throughout this article), the spatial resolution of the SWP is 300 pc per line, which much larger than the bulk of the line emitting region in NGC 3516. Therefore,

the emission-line region, as well as the dominant nonstellar continuum, is detected as a point source and the use of a Gaussian fit is justified.

Both the SWP and LWP data are corrected for the slight temperature dependency of the detector sensitivity. The LWP data were calibrated with the standards obtained in 1984-1985 (Cassatella, Lloyd, & Riestra 1988). The May 1980 flux calibration was used for the SWP data. The accuracy of this calibration is estimated at ~10% (Bohlin & Holm 1980), but work by Finley et al. (1990) suggests that the actual calibration could be up to 20% different from the May 1980 calibration.

The photoelectric data in the Fine Error Sensor (FES) on board the *IUE* were converted to V-band magnitudes and listed in Table 1. The formal statistical error due to the calibration is ±0.07 mag (Sonneborn et al. 1987). The field of view of the FES has a diameter of 12″ while NGC 3516 extends 2.′1 by 1.′8, therefore only the central emission region is detected.

3. RESULTS

3.1. The Short-term UV Variability

From these spectra, we calculated the average fluxes in the continuum intervals and estimated the errors by using the standard deviation of the data points in the continuum interval. These errors might underestimate the true error, as the uncertainty in the calibration is not taken into account. The continuum was studied for variability by fitting the data points with the average flux (shown in Figure 3 as the dashed lines). A change in continuum level is obvious between October 7 and 9 (day 281 and 283, respectively). Averaged over wavelength the change is 16% (the ratio varies from 88% ± 8% around 1710 Å to 81% ± 5% around 1955 Å). The statistics of the test for variability on the whole data set are shown in Table 2, which indicates significant variability at the 99.6% level in the most sensitive (1940-1970 Å) part of the SWP.

The variability comes from the Oct. 7 data, since exclusion of this day results in no significant variability (Table 3), with goodness-of fit parameter q close to 1. An upper limit on the variability excluding Oct. 7, conservatively estimated from the 1σ error estimates on the fluxes, is found to be $\pm 6\%$ around 1955 Å and $\pm 7\%$ around 3000 Å on a timescale from days up to a week. The power law index of the combined SWP and LWP continuum showed no significant variations from the mean either.

On average, the V magnitude was 12.31 on October 7 and 12.41 between October 9 and 16; a small initial decrease and a constant optical brightness afterwards, consistent with the decrease detected in the UV continuum between October 7 and 9 and the steady ultraviolet flux level between October 9 and 16. The decrease in the UV is about 0.2 mag, while the optical decrease is only 0.1 mag.

3.2. Emission Lines

We coadded the spectra to study the emission lines. The measured line properties are listed in Table 4 and the lines are identified in Figures 1. The Lyα emission line could not be measured, as the blue wing is blended with the geocoronal Lyα line and the red wing with the strong N V absorption and possibly the N V emission as well. Following Ulrich and Boisson (1983) we measured the intensities of the emission features, uncorrected for interstellar absorption, absorption lines (also for C IV) or line blends. In Table 4 we list the formal errors, where the error (relative to the flux) in the individual line emission data point is approximated by the relative σ in the continuum bin bordering the emission line. The major source of error in the line measurements is the uncertainty in the continuum level, which is contaminated by the broad wings of the emission lines, Galactic absorption lines, and blended Fe II line and Balmer continuum emission. Therefore, the formal error seriously underestimates the actual error in the line measurements.

These 1989 UV line measurements can be compared to the ones reported by Ulrich and Boisson (1983) obtained from 1981 spectra. Very good agreement was found for the

strong, low excitation lines (C III], Si III], and Mg II) and the weak lines (N IV, O III], and N III]). However, the reported O III λ3133 line was not found; we established an upper limit at 25% of the flux listed by Ulrich and Boisson. Also, different results were found for the strong, high excitation lines (Si IV, O IV, and C IV): these line fluxes were much lower, which could be accounted for by the significantly stronger absorption features found in these emission lines. Compared to the 1981 spectrum the absorption is much stronger in the C IV, N V, and Si IV, O IV lines.

The ratio of C III]/C IV measured in NGC 3516 is 0.19. This is a very conservative upper limit as there is flux from Si III] included in the C III] measurement and the C IV is severely underestimated due to the strong absorption. Such a low ratio is exceptional for quasars or Seyfert 1 galaxies (Kwan and Krolik 1981) and as this ratio is used to set an upper limit on the density in the BLR. A ratio $\ll 0.19$ would allow for high densities ($n_e \gtrsim 10^{10}$ cm^{-3}). The strength of Si III] relative to C III] is expected to increase with higher densities as well (Rees, Netzer, & Ferland 1989).

3.3. Galactic Absorption Lines

We measured the absorption lines listed in Table 5 and indicated by tick marks in Figure 1. All these lines arise from low-ionization species. There are also strong absorption features close to the redshifted emission lines of N V and C IV. These absorption lines are associated with material within the NGC 3516 system. Considering the wavelength of the Si IV $\lambda\lambda$1393,1402 absorption doublet (λ_{abs} are 1403$\pm$1 and 1412$\pm$2 Å) This feature is also thought to arise in the Seyfert and not in our Galaxy. In contrast, the Mg II line is centered very close to the rest wavelength and therefore attributed to Galactic absorption.

3.4. The C IV, N V, and Si IV Absorption Features

We measured the equivalent width of the CIV, N V, and Si IV absorption lines and listed the results in Table 6. The errors listed for the line measurements are again formal,

and therefore lower limits to the true errors. Following VSB, the equivalent width of CIV was measured in two ways: first by joining the two peaks by a straight line and second, by fitting a Gaussian profile to the narrow emission line components (as the narrow-line profile in QSOs is approximated well by a Gaussian). The first method undoubtedly underestimates the true equivalent width, while the second method is highly uncertain in its speculative fit of the emission profile. The Gaussian fit peaks around 1555 Å and not around the expected emission peak of 1564 Å. There is evidence that the base of the emission feature is also blueshifted with respect to the systemic velocity and that the absorption feature is not shifted considerably compared to the C IV emission line profile (VSB). The N V line was fit by a horizontal line to its red emission peak and the Si IV by a straight line to its red and blue peak. The Si IV line is weak and is hard to measure accurately in the relatively strong noise.

The overall C IV line profile is remarkably symmetric, which is exceptional as most C IV profiles in NGC 3516 are distinctly asymmetric with a stronger red than blue peak (VSB). Compared to the observations from 1978 to 1984, the 1989 continuum is at a high level, while the peaks of the C IV line reach the highest flux levels ever. The C IV absorption equivalent width is also very strong, measured either way, and the N V equivalent width is unsurpassed.

There is an absence of significant variability in the October 1989 absorption measurements (Table 6). The height of the peaks deviated only for the blue peak on October 9. This also accounts for the smaller equivalent width under the straight line fit found on that date. The equivalent widths of C IV (under the Gaussian fit) and N V showed no variation within their formal errors, thus certainly excluding significant variability. In this light, we are justified to coadd the spectra and study the absorption features in the coadded spectrum. The coadded spectrum has a total exposure time of 1260 minutes (far more than any earlier coadded spectrum studied; VSB, Walter et al. 1990), resulting in spectrum with an unequalled signal-to-noise ratio.

3.5. Lower Limit on the Carbon Column Density

We measured the optical depth τ derived from the ratio of the observed flux to the estimated, unabsorbed flux:

$$\tau = -\ln(F_\nu / F_\nu^{\rm unabs}).$$

Again we approximate the unabsorbed profile with a straight line and a Gaussian fit to the narrow line component. This calculation is only correct (Barlow, Junkkarinen, and Burbidge 1989) if there is no scattered light and emission from the absorption line region; if the absorption line does not contain any unresolved narrow lines; and if the absorber covers the emitting source. The spectral resolution of the SWP camera is low, so any unresolved narrow lines cannot be excluded with certainty. VSB showed that the absorbing region must cover (at least partially) the line emitting region and the continuum. Together with the uncertainty of the unabsorbed line profile, this estimate of the optical depth is therefore slightly uncertain. The optical depth reaches values slightly greater than 1 in the line center. C IV absorption ranges from $\sim$ 0 km s^{-1} to $\sim$ -3000 km s^{-1}. The absorption peaks around -1000 km s^{-1}. The C IV absorption falls off more rapidly on the red than the blue side and there is evidence (e.g., on October 16) that the absorption profile flattens out around the minimum. The N V absorption also sets in around the redshifted rest wavelength and reaches a minimum around -1000 km s^{-1}, but extends to at most ~ -3000 km s^{-1}.

The column density of C^{3+}, $N_{C^{3+}}$, can be estimated from the optical depth (Lucy 1971) using the method by Junkkarinen, Burbidge, and Smith (1983):

$$N_{C^{3+}} \geq \left(\frac{\nu_0 mc}{f\pi e^2}\right) \int \tau \, d(\ln\lambda),$$

where ν_0 is the rest frequency, and f the oscillator strength. Considering the uncertainty in τ we can only determine a lower limit to $N_{C^{3+}}$. It is at least 2.2×10^{15} cm^{-2} for the Gaussian fit, and 1.8×10^{15} cm^{-2} for the straight line fit. Such $N_{C^{3+}}$ would correspond to $N_{\rm H} \geq 2 \times 10^{19}$ cm^{-2}, assuming cosmic abundances and that 1/3 of all carbon is three

times ionized. VSB estimated a similar lower limit to $N_{C^{3+}}$ of $\sim 10^{15}$ cm^{-2} using the curve of growth method.

3.6. Estimate of the Distance from the Absorber to the Continuum Source

Continuing on the assumption that photoionization is the main ionization mechanism in the absorbing region, we can relate the ionization parameter U to n_e, the density of the absorber, r, the distance from the absorber to the continuum source, in addition to observable quantities. For U we use the value at which the fractional abundance of C^{3+} peaks, U_p, as large deviations from this value are not expected considering the obvious strength of the C IV features. Smith and Penston (1988) calculated U_p with the photoionization code CLOUDY and $\alpha = 1.5$. For $\log N_H = 20$, 21, and 22, they find $\log U_p = -2.18$, –1.65, and –0.83, respectively. This would give us in the case of NGC 3516 and $\log N_H = 20$, $n_e r^2 \sim 2 \times 10^{43}$ cm^{-1}, or with n in 10^5 cm^{-3} and r in pc: $r_{pc}^2 \sim 20/n_5$. For $\log N_H = 21$ and 22, $r_{pc}^2 \sim 6/n_5$ and $1/n_5$, respectively.

3.7. Variability in the Continuum and Absorption

NGC 3516 is variable, both in the continuum and absorption. Such variability has been reported for other Seyferts as well; in particular, NGC 4151 shows absorption in C IV which changes in equivalent width and wavelength with time (Clavel et al. 1987). Variability can be attributed to either ionization changes in the absorber or changes in the bulk motion of the absorber in the line of sight. Boroson et al. (1991) reported on the appearance of a new absorption system in Mkn 231, which these authors explained by motion of an absorbing cloud into the line of sight. Mkn 231 differs from NGC 3516 in the fact that it is not as highly ionized. We will show that the variability of NGC 3516 can readily be explained to be due to changes in the ionization of the absorber.

We retrieved all the *IUE* archival data (up to 1989) and extracted these with the Gaussian routines as described above. The data obtained with the old software (before

1980) were reprocessed with the corrected ITF. We searched the archival data for variability on the shortest timescale. To follow the actual change in the continuum and C IV absorption, observations taken frequently are required. Observations taken in 1984 showed the fastest change in the shortest period (see also VSB and Walter et al. 1990). Definite variability in both the continuum flux level and equivalent width of the C IV absorption was found on a time scale of about a week. In this episode, anticorrelation of the continuum flux and C IV equivalent width, as reported by VSB, was seen. Between October and November, the continuum flux decreased, while the absorption in C IV became stronger.

In theory, if the absorbing region is in photoionization equilibrium, then the fractional abundance of C^{3+} first increases with U, reaches a peak value, $U_{\rm p}$, and then decreases with the ionization parameter. In 1984, the continuum flux decreased, resulting in a smaller U. If we assume that the changes in the absorbing strength result from changes in the fractional abundance (which, in turn, is caused by the time variability of the continuum source), then an increase in the C IV equivalent width would correspond to an increase in the fractional abundance of C^{3+}. This, together with the decreasing U implies that $U > U_{\rm p}$. The lower limit to U corresponds to an upper limit on $n_5\, r_{\rm pc}^2$. VSB inferred a lower limit for the density from the observed upper limit on the recombination time $t_{\rm rec}$ during the 1984 epoch: $n_5 \sim 10/t_{\rm rec} \sim 1$ (with $t_{\rm rec}$ in days). Together with $r_{\rm pc}^2 \lesssim (20/n_5)$ derived above, this would lead to an upper limit to r of 5 pc assuming log $N_{\rm H}$= 20 (for log $N_{\rm H}$ = 21 and 22, r would be $\lesssim$3 and $\lesssim$1 pc, respectively).

Smith & Penston (1988) also predicted the correlation properties between the absorption from C IV, N V, and Si IV. Roughly, the absorption strength of N V and Si IV vary with C IV (VSB). However, it is difficult to assess whether there is a significant correlation with the C IV absorption: the Si IV feature is very weak, but appears to be correlated, while the stronger N V line deviates from a possible correlation during several epochs (see Figure 9 of Walter et al.). This is unfortunate, as the correlations and anti-correlations could constrain the ionization parameter further.

4. DISCUSSION

4.1. A Comparison with BAL QSOs

There is a class of QSOs, the Broad Absorption Line QSOs, which has much in common with NGC 3516 and could very well be considered to be its high luminosity, high redshift equivalent. Since most observed BAL QSOs have large redshifts ($z \gtrsim 1$), they have been studied extensively at high resolution ($\sim$ 1 Å) with optical telescopes. The BAL profile can be highly structured with multiple troughs. In comparison, the nearby galaxies exhibiting such absorbing features have been observed with *IUE* and display smooth absorption profiles, but these could be attributed to the low resolution and a structured profile cannot be excluded.

The most obvious similarity between NGC 3516 and the BAL QSOs is the absorbing feature in the high ionization lines: C IV, N V, and Si IV. There are BAL QSOs with absorption in low-ionization lines (e.g., Mg II), but they are the exception to the rule. The most striking difference is the strength of the absorption line: the equivalent width is $\sim$40 Å in the BAL QSOs and at most 10 Å in NGC 3516. The range in velocity is also quite different: from $\sim$ 0 to at least $\sim$ 10,000 km s^{-1} in BAL QSOs and from $\sim$ 0 to $\sim$ 3500 km s^{-1} in NGC 3516. Variability has been reported for both NGC 3516 and several BAL QSOs, only the timescale differs considerably: NGC 3516 varies on a timescale of months if not weeks, while BAL QSOs have been reported to vary on a timescale of years.

Based on the failure to detect broad [O III] emission (which is expected to arise in the BAL region through collisional excitation) in the nearby BAL QSO PG 1700+518, Turnshek et al. (1985) constrain n_e to be larger than the critical density for de-excitation (6×10^5 cm^{-3}), unless the covering fraction of the absorber is very small ($q \lesssim 0.05$, which is not in agreement with the assumption that all QSOs have BAL regions). With a similar argument as presented above, this implies that the absorbing gas is located around $r \lesssim 30$ pc in PG 1700. Assuming that the physical conditions are similar in NGC 3516 and

making use of the fact that this limit scales with the square root of the luminosity, this would correspond to an upper limit for NGC 3516 comparable to the one derived above:

$$r = \left(\frac{L_{3516}}{L_{1700}}\right)^{1/2} r_{1700} \leq (6.3 \times 10^{-3})^{1/2} \times 30 \leq 2\,\mathrm{pc},$$

where the subscripts 3516 and 1700 refer to NGC 3516 and PG 1700+518, respectively).

A lower limit to r in BAL QSOs is derived from the fact that Lyα is occulted by the N V absorption, implying that the BAL clouds are outside the Lyα emitting region, i.e. $r \gtrsim 1$ pc. A similar argument can be made for NGC 3516, where the absorbers have to be located outside the region where the C IV and broad Lyα emission originates (but not necessarily outside the C III] and Mg II emitting region). In the case of NGC 4151 there is evidence for a stratified emission region, with the core of the C III] emission line originating far outside the C IV line region (Clavel et al. 1990). In the case of NGC 3516, similar studies of the emission line variations (Edelson, Krolik, and Pike 1990) did not give significant estimates on the emission line region, let alone on its stratification. However, this could be attributed to the uneven and undersampling of the observations of NGC 3516, and it is not unrealistic to assume a stratified emission region for NGC 3516. This would put the absorber outside the C IV emitting region, i.e., $r \gtrsim 25$ lt-days (0.02 pc). NGC 4151 has a similar luminosity as NGC 3516 and therefore the estimates for the emission region derived in NGC 4151 can be applied directly to NGC 3516. Recent high-rate reverberation studies of NGC 4151, both optically and with *IUE*, also showed that the BLR is much smaller than previously thought: $r \lesssim 21$ lt-days for the Balmer lines (Maoz et al. 1991) and $r \lesssim 7$ lt-days for the C IV line (Clavel et al. 1990). This will decrease the lower limit on r even further to $\gtrsim 0.005$ pc.

Next we address the fact that the absorbing features are weaker and narrower in NGC 3516 compared to the BAL QSOs. In a first approximation, this can be attributed to the much lower luminosity in NGC 3516 which cannot accelerate the absorber to the

high velocities seen in BAL QSOs, resulting therefore in absorption features with smaller equivalent widths and narrower breadths. We can envision two simple models:

1. The radiative acceleration is the dominant force acting on the absorbing clouds. The terminal velocity v of the absorbing clouds which are accelerated from a starting distance $r_{\rm min}$ scales as $(L/r_{\rm min})^{1/2}$ (Weymann, Turnshek, & Christiansen 1985, hereafter WTC). For BAL QSOs $r_{\rm min} \sim 10$ pc for intermediate velocities and $r_{\rm min} \sim 1$ pc for the high-velocity clouds. In particular, in the case of QSO 1303+308 (Foltz et al. 1987) a similar argument led to an estimate of $r_{\rm min} \sim 3$ pc for the high velocity clouds ($v \sim 10,000$ km s^{-1}). This would correspond to a terminal velocity in NGC 3516 of

$$\left(\frac{L_{Q1303}}{L_{N3516}}\right)^{-1/2} \left(\frac{r_{\rm min,N3516}}{r_{\rm min,Q1303}}\right)^{1/2} v_{\rm Q1303} \sim (3200)^{-1/2} \times (3/0.01)^{1/2} \times 10,000 \sim 3000 \ {\rm kms}^{-1}.$$

   Associating the clouds, which have been accelerated from the minimum distance and have reached the maximum velocity, with the blue edge of the absorbing feature, we find terminal velocities of at least 3000 km s^{-1} in NGC 3516, in good agreement with the scaled down version of a BAL QSO.

2. The acceleration is due to a wind, in which ram pressure is the dominant force. WTC noted that the observed profile of the BAL, with a sharp red edge and a slowly rising blue edge, could easily be interpreted as arising from the line of sight passing through the main clouds in addition to smaller clouds which have been torn off the main clouds and accelerated to higher velocities. NGC 3516 shows a similar profile in the sense that the red edge is steeper than the blue edge (Figures 1 and 2). The terminal velocity scales similar to the radiative acceleration, but the velocities are expected (for similar L and $r_{\rm min}$) to be larger by a factor $\sim$10 (WTC). Thus, the clouds are more efficiently accelerated by a wind than by radiation and therefore the clouds in the wind model can originate at larger distances. For this reason, and for the need to invoke a confining medium for the radiatively accelerated clouds, the wind model is favoured in BAL QSOs. The wind model is equally applicable in NGC 3516, allowing for the high velocity clouds to originate at

moderate distances and the intermediate velocity clouds (the majority as the absorption clearly peaks around ~1000 km s^{-1}) to originate closer to the continuum source. The same problems which plague these acceleration models in BAL QSOs will have to be addressed for NGC 3516, e.g., the existence of the wind, and the instabilities of the clouds (WTC). VSB found evidence for the presence of a wind in NGC 3516: the C IV profile change in a two week period displayed a P Cygni form, indicating radial outflow of the UV absorbing gas. Also, Goad & Gallagher (1987) found optical evidence for outflow with velocities of $\sim$ 700 km s^{-1}, on a scale of 100 pc.

4.2. The X-ray – UV Connection

Since the X-ray continuum source is smaller than the UV source, and as the UV absorbers are (at least partially) covering the continuum, the material producing the UV absorption could be expected to produce the X-ray absorption as well. If the UV and X-ray absorption had been observed to be well correlated, then there would have been strong evidence that one component is responsible for both types of absorption. Unfortunately, neither the UV nor the X-ray absorption was found to vary during our simultaneous observations in 1989 and this correlation could not be established.

There are at least a dozen AGN which have been observed with *IUE* and which display UV absorption features of intrinsic origin (i.e., not of intergalactic or Galactic origin; Ulrich 1988, Kinney et al. 1990). Some are genuine BAL QSOs, others are nearby galaxies very similar to NGC 3516. Most have strong and variable X-ray emission ($N_{\rm H} \sim 10^{22}$ cm^{-2}), but there are galaxies with no larger $N_{\rm H}$ than expected for Galactic absorption (e.g., MCG 8-11-11). If the column density is close to the lower limit derived for NGC 3516, i.e. $N_{\rm H} \sim 10^{20}$ cm^{-2}, observable UV absorption lines could be produced, but the X-ray absorption would be difficult to detect. Therefore, the presence of UV absorption lines together with the absence of substantial X-ray absorption, does not rule out that the UV absorption arises in the same location as the X-ray absorption (e.g., in the broad line region

as suggested by Reichert, Mushotzky, and Holt 1986). Nevertheless, there are highly X-ray absorbed galaxies which do not show any evidence for absorption in the UV. A complete study of the X-ray and UV absorption properties galaxies like NGC 3516 and BAL QSOs has not yet been undertaken. Therefore, it is too early to conclude from the absorption properties of AGNs in the UV and X-ray that these arise in the same location and through the same process.

In our Ginga spectra of NGC 3516, as in other observations of Seyfert 1 galaxies (Piro, Yamauchi, & Matsuoka 1990), we found evidence for two absorption components: the 'standard' cool absorption with $N_{\rm H} \sim 10^{22.6}$ cm^{-2}, and the very thick cool absorber with $N_{\rm H} \sim 10^{24.6}$ cm^{-2}. Alternatively, the second component can be interpreted to arise through reflection from very thick cool matter ($N_{\rm H} \gtrsim 10^{25}$ cm^{-2}; Lightman & White 1988). Either way it suggests the presence of dense material in the Seyfert galaxy. If the UV and X-ray absorption have the same origin, with which X-ray component is the UV absorption associated? Obviously, if the hard tail above 7 keV arises in a reflective slab, no absorption is expected, but the X-ray observations do not allow us to distinguish between this model and the very thick cool absorber alternative. Assuming that two X-ray absorbers are present, a thin and thick one, which could be responsible for the UV absorption? The *IUE* observations established a lower limit on $N_{\rm H}$ of $\sim 10^{20}$ cm^{-2}, allowing both components.

We will show that the thick X-ray absorption could arise in a small number (~ 30) of dense clouds, which would also be responsible for the UV absorption. Invoked by the small BLR sizes found recently through reverberation studies, high-density models for the broad line clouds have been calculated (Rees, Netzer, & Ferland 1989; Ferland and Persson 1989), which show that for densities around $10^{11} - 10^{12}$ cm^{-3}, C IV would be stronger than thought previously for the standard, low density BLR models. The same is true for Si IV and NV, the other lines which are seen in absorption. The lack of Mg II λ 2798 absorption is more difficult to explain. Its strength peaks around 10^{10} cm^{-3} and levels off at higher densities faster than C IV, but still remains at considerable intensity.

Specifically, comparing the relative line intensities at 10^{10} cm^{-3} and 10^{12} cm^{-3} (for model A of Rees, Netzer, & Ferland 1989), the C III] line decreases by 90%, C IV increases by 7%, N V increases by a factor of 7, and Mg II decreases by 45%. If the absorption regions are highly ionized, little Mg^{+} would be expected, while C^{3+} and N^{4+} would be abundant. This is illustrated by the model in which the ionization parameter is allowed to vary (model D,Figure 3 of Rees, Netzer, & Ferland 1989). Mg^{+} and C^{2+} diminish quickly with increasing ionization, while Si^{3+} and C^{3+} decrease slowly. Thus, the absence of the low-ionization species can be used to constrain the ionization parameter U. In the model of Smith & Penston (1988), this implies $U > 0.006$ and $U > 0.05$ for $\log N_{\rm H} = 21$ and 22, respectively. Our estimates of the lower limit to U fulfill this inequality (§3.7). Some care has to be taken with the interpretation of the emission line models to predict the absorption line properties. While there can be little doubt that the high-ionization species (like C^{3+}) are present in such high-density broad line clouds, these might be expected at the side illuminated by the continuum source. In order for absorption to take place in the same broad line clouds, the absorber has to be located further away from the high-ionization front. It might be difficult to achieve the right ionization level there as the photoionization flux will be absorbed by the intervening dense material. The same argument holds if the UV absorption is only due to the outer broad line clouds, as the intervening clouds will intercept the ionizing flux.

As pointed out by VSB, in the standard broad-line cloud model at least 30 clouds are needed to achieve the observed width in the absorption lines, as the thermal velocity dispersion in a single cloud is small. The $N_{\rm H}$ of a standard dense cloud is $\sim 10^{23}$ cm^{-2}, therefore 30 clouds will result in the observed X-ray column density of $10^{24.6}$ cm^{-2}. These clouds will have to be located quite close to continuum source. The ionization parameter increases with $N_{\rm H}$ and if we (as a rough estimate) extrapolate this trend as calculated by Smith & Penston (1988) to $\log N_{\rm H} = 24$, then $\log U_{\rm p} \sim 0.4$. Following the same argument as above, this gives $r \lesssim 0.3$ pc. Walter et al. (1990) argue that the UV absorber

is located in a single cloud. This will be difficult to achieve: in order to obtain the required width in the absorption line from one cloud, the internal velocity dispersion has to be enormous. Such a cloud would not be stable. Walter et al. arrived at the single cloud model from the fact that nine consecutive observations followed two (anti)correlations between the absorption strength and the continuum flux. However, seven observations do not follow these correlations. It is therefore difficult to maintain that the trend of decreasing absorption strength with increasing continuum flux has to be explained with the presence of a single cloud.

5. CONCLUSIONS

In conclusion, NGC 3516 has the characteristics of a low luminosity BAL QSO. The density of the absorbing region has a similar lower limit in this Seyfert as in the BAL QSOs. The absorber of C IV, N V, and Si IV is probably located between 0.01 and 5 pc in NGC 3516, much closer to the nucleus than in the high luminosity BAL QSOs. The clouds in NGC 3516 do not reach the large velocities and distances from the continuum source as in BAL QSOs, because the central engine in NGC 3516 can only accelerate them to moderate velocities. Therefore, the range of velocities and the maximum velocities are smaller, resulting in an absorbing feature which is narrower with a smaller blueshift in the rest frame of the Seyfert.

Our simultaneous observations in the UV and X-ray are not in disagreement with the assumption that the UV absorber is also responsible for the X-ray absorption. This absorption could be identified with the dense component ($N_{\rm H} \sim 10^{24.6}$ cm^{-2}), detected in the Ginga observations. If so, then the absorber would be located very close to the continuum source: $r \lesssim 0.3$ pc. The lack of Mg II absorption could be attributed to the high ionization level of the absorbing region.

6. CONTINUING AND FUTURE WORK

There are two uncertainties which limit the usefulness of the current measurements of absorbing columns of C IV, N V, and Si IV. One is the shape of the unabsorbed continuum plus line emission. The other is the profile of the absorption features. The latter can be studied better with high resolution observations. Such observations for high z BAL QSOs showed a structured, detailed absorption through, in contrast to the profiles obtained with *IUE*. Such BAL profiles have been interpreted to arise from a large (possibly up to $\sim 10^3$) ensemble of clouds. It would be very useful to estimate the number of absorbing clouds in NGC 3516. Even a continuous absorbing medium such as a wind cannot be excluded based on the *IUE* data. More importantly, high resolution data would allow accurate measurements of the absorbing columns; an improvement over the lower limits which can be established with the *IUE* data. If the absorbing column could be constrained to low values ($\sim 10^{20}$ cm^{-2}), then the high density clouds are probably ruled out as a location for the absorber: a single cloud would exceed the absorbing column, while it would produce a absorption feature which is far narrower than observed.

Further analysis of archival IUE data on NGC 3516 spanning the 1978-1988 period is also under way, again using the Gaussian extraction routines. We will investigate the reported P Cygni profile for the absorption line variations. Also, an attempt will be made to measure the absorption properties of the Mg II emission line, which has not been reported in the literature. The Mg II line can be used to put better contraints on the total column density of the absorbing gas, since it samples the neutral parts of the clouds which are behind the illuminated faces, and which are supposed to comprise the bulk of the standard broad-line clouds.

Although the X-ray spectrum did not exhibit changes in absorbing column density during this brief monitoring period, the X-ray flux and spectral shape did vary in a complex manner. A paper describing the simultaneous *IUE* and Ginga observations is in preparation.

TABLE 1
IUE OBSERVATIONS OF NGC 3516

Image #	Int. time (min.)	Date	m_V
SWP 37274	100	1989 Oct 7	12.27
SWP 37275	250	1989 Oct 7	12.34
SWP 37293	330	1989 Oct 9	12.40
LWP 16524	65	1989 Oct 10	12.43
SWP 37308	345	1989 Oct 12	12.42
LWP 16548	60	1989 Oct 12	12.39
SWP 37327	335	1989 Oct 16	12.42
LWP 16567	60	1989 Oct 16	12.39
SWP 37398	140	1989 Oct 19	–
LWP 16573	60	1989 Oct 19	–

TABLE 2
SHORT-TERM UV VARIABILITY
(1989 October 7 - 16)

λ (Å)	$< f >$ (mJy)	χ^2	q	variability[a] (% of $< f >$)
1335-1360	1.39	4.6	.336	27
1435-1470	1.57	7.4	.114	30
1690-1730	2.06	7.8	.095	23
1800-1842	2.34	10.0	.040	21
1940-1970	2.61	15.5	.004	22
α^b	1.75^b	1.11	.891	26

[a] upper limit on the variability relative to $< f >$
[b] power law index of the SWP continuum fit ($F_\nu \propto \nu^{-\alpha}$).

TABLE 3
SHORT-TERM UV VARIABILITY
(1989 October 9 - 16)

λ (Å)	$< f >$ (mJy)	χ^2	q	*variability*[a] (% of $< f >$)
1335-1360	1.32	1.73	.420	20
1435-1470	1.49	0.72	.696	13
1690-1730	1.97	0.64	.727	10
1800-1842	2.27	1.02	.602	8
1940-1970	2.51	0.09	.954	6
2655-2720	4.68	0.86	.649	10
2960-3035	6.07	0.02	.991	7
α[b]	1.91[b]	0.45	.800	7

[a] Upper limit on the variability relative to $< f >$.
[b] Power law index of the *IUE* (SWP+LWP) continuum fit ($F_\nu \propto \nu^{-\alpha}$).

TABLE 4
EMISSION-LINE MEASUREMENTS

ID[a]	Intensity[b]	EW[c]
Si IV λ1397, O IV λ1407	16.4±1.8	7.2±0.8
N IV] λ1484	4.7±0.9	1.9±0.4
C IV λ1549	185.6±3.3	83.7±2.4
He II λ1640	17.8±1.0	7.8±0.5
O III] λ1663	3.2±0.5	1.5±0.3
N III] λ1750	3.6±0.5	1.7±0.3
C III] λ1909, Si III] λ1892	35.6±0.7	16.9±0.4
Mg II λ2798	69.0±2.2	35.2±1.3
O III λ3133	<3.5±1.7	<1.7±0.9

[a] Identification of emission line and rest wavelength.
[b] Observed flux in 10^{-14} ergs cm^{-2} s^{-1}.
[c] Observed equivalent width in Å.

TABLE 5
GALACTIC ABSORPTION-LINE MEASUREMENTS

ID	λ_{min} (Å)	EW (Å)
O I λ1302, Si II λ1304	1302±2	0.7±0.2
C II λ1335	1334±1	0.7±0.2
Fe II λ2586	2587±3	1.3±0.4
Fe II λ2599	2602±3	1.5±0.3
Mg II λλ2796, 2803	2797±3	1.9±0.3

TABLE 6
1989 ABSORPTION MEASUREMENTS

line parameter	Oct 7[e]	Oct 9	Oct 12	Oct 16
1450 Å continuum[a]	2.67±0.24	2.18±0.20	2.25±0.21	2.05±0.13
2700 Å continuum[a]	-	1.91±0.12	1.99±0.10	1.84±0.12
C IV blue peak flux[a]	6.93	5.76	6.66	6.55
C IV red peak flux[a]	6.91	6.76	6.74	6.85
C IV blue peak wavelength[b]	1542	1542	1541	1546
C IV red peak wavelength[b]	1565	1567	1567	1566
C IV minimum absorption wavelength[b]	1557	1560	1557	1556
C IV EW[c]	8.2±0.4	7.1±0.2	8.9±0.4	8.1±0.4
C IV EW[d]	10.4±0.3	10.1±0.3	10.8±0.3	9.6±0.3
N V λ1240 EW	7.3±0.2	7.2±0.2	6.8±0.2	7.1±0.2
Si IV λ1393 EW	2.9±0.4	3.2±0.4	3.6±0.4	4.4±0.2
Si IV λ1402 EW	1.0±0.3	1.8±0.3	2.1±0.3	1.8±0.3

[a] Observed flux in 10^{-14} ergs cm^{-2} s^{-1} $Å^{-1}$.
[b] Observed wavelength with an error of ~1 Å.
[c] Observed equivalent width (Å) under straight line between the peaks.
[d] Observed equivalent width (Å) under a Gaussian fit to the narrow line component (FWHM~30 Å).
[e] SWP37275 only as SWP37274 has a cosmic ray hit at the red peak of C IV; no LWP spectrum obtained on this date.

REFERENCES

Barlow, T. A., Junkkarinen, V. T., & Burbidge, E. M. 1989, *Ap. J.*, **347**, 674.

Bohlin, R. C., & Holm, A. V. 1980, NASA *IUE* Newsletter, **10**, 37.

Boroson, T. A., Meyers, K. A., Morris, S. L., & Persson, S. E. 1991, *Ap. J. (Letters)*, **370**, L19.

Clavel, J. et al. 1987, *Ap. J.*, **321**, 251.

Clavel, J. et al. 1990, *M.N.R.A.S.*, **246**, 668.

Cassatella, A., Lloyd, C., & Riestra, R. G. 1988, NASA *IUE* Newsletter, **35**, 225.

Edelson, R. A., Krolik, J. H., & Pike, G. F. 1990, *Ap. J.*, **359**, 86.

Ferland, G. J. & Persson, E. 1989, *Ap. J.*, **347**, 656.

Finley, D. S., Basri, G., & Bowyer, S. 1990, *Ap. J.*, **359**, 483.

Foltz, C. B., Weymann, R. J., Morris, S. L., & Turnshek, D. A. 1987, *Ap. J.*, **317**, 450.

Goad, J. W., & Gallagher III, J. S. 1987, *A. J.*, **94**, 640.

Halpern, J. P. 1982, Ph.D. thesis, Harvard University.

Halpern, J. P. 1984, *Ap. J.*, **281**, 90.

Junkkarinen, V. T., Burbidge, E. M., & Smith, H. E. 1983, *Ap. J.*, **265**, 51.

Kinney, A. L., Bohlin, R. C., Blades, J. C., & York, D. G. 1991, *Ap. J. Suppl.*, **75**, 645.

Kwan, J., & Krolik, J. H. 1981, *Ap. J.*, **250**, 478.

Lucy, L. B. 1971, *Ap. J.*, **163**, 95.

Lightman, A. P., & White, T. R. 1988, *Ap. J.*, **335**, 57.

Maoz, D. et al. 1991, *Ap. J.*, **367**, 493.

Piro, L., Yamauchi, M., & Matsuoka, M. 1990, *Ap. J. (Letters)*, **360**, L35.

Reichert, G. A., Mushotzky, R. F., Petre, R., & Holt, S. S. 1985, *Ap. J.*, **296**, 69.

Rees, M. J., Netzer, H., & Ferland, G. J. 1989, *Ap. J.*, **347**, 640.

Reichert, G. A., Mushotsky, R. F., Holt, S. S. 1986, *Ap. J.*, **303**, 87.

Smith, L. J., & Penston, M. V. 1988, *M.N.R.A.S.*, **235**, 551.

Sonneborn, G., Oliversen, N. A., Imhoff, C. L., Pitts, R. E., & Holm, A. V. 1987, *IUE* Observing Guide, p. 46.

Turnshek, D. A., Foltz, C. B., Weymann, R. J., Lupie, O. L., McMahon, R. G., & Peterson, B. M. 1985, *Ap. J. (Letters)*, **294**, L1.

Ulrich, M. H., & Boisson, C. 1983, *Ap. J.*, **267**, 515.

Ulrich, M. H. 1988, *M.N.R.A.S.*, **230**, 121.

Urry, C. M., & Reichert, G. 1988, NASA *IUE* Newsletter, **34**, 95.

Voit, G. M., Shull, J. M., & Begelman, M. C. 1987, *Ap. J.*, **316**, 573 (VSB).

Walter, R., Ulrich, M. H., Courvoisier, T. J. L., Buson, L. M. 1990, *Astr. Ap.*, **233**, 53.

Weymann, R. J., Turnshek, D. A., & Christiansen, W. A. 1985, in *Astrophysics of Active Galaxies and Quasi-stellar Objects*, ed. J. S. Miller (Mill Valley: University Science Books), p. 333 (WTC).

FIGURE CAPTIONS

FIG. 1. – Coadded spectrum of NGC 3516 obtained with *IUE* in 1989. Data points flagged with X's are affected by cosmic ray hits and the presence of reseaux. The emission lines are indicated at the laboratory wavelengths redshifted with $z = 0.009$. The strong emission line around 1216 Å is geocoronal Lyα. The tick marks under the graph indicate probable Galactic absorption lines. The absorption features shortward of the N V and C IV lines are associated with the Seyfert itself. Considering the wavelengths of the absorption around 1400 Å, these features are also thought to be associated with NGC 3516 and not Galactic.

FIG. 2.– Individual spectra of NGC 3516 obtained in 1989. Note the lack of significant changes, except that the overall flux level on October 7 is higher than the others.

FIG. 3.– Short-term variability of the ultraviolet continuum emission for the spectra obtained in 1989 October. The dashed line indicates the error-weighted average flux. The first set includes all the observations (see also Table 2), while the second set excludes October 7 (Table 3). Note the absence of significant variations at all wavelengths and the constancy of the power law index.

Figure 1

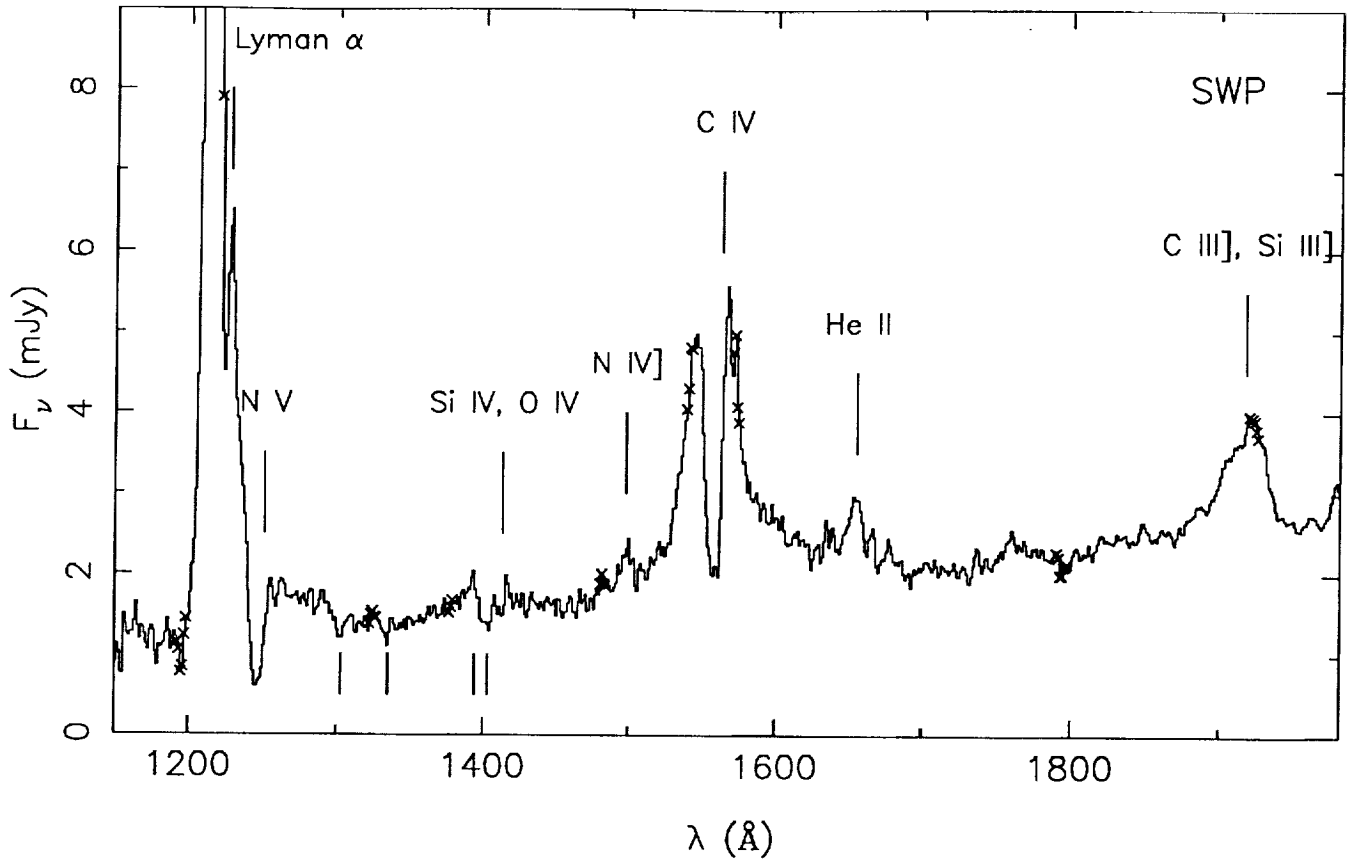
Lyman α
SWP
C IV
C III], Si III]
He II
N IV]
N V
Si IV, O IV
F$_\nu$ (mJy)
λ (Å)
0
2
4
6
8
1200
1400
1600
1800

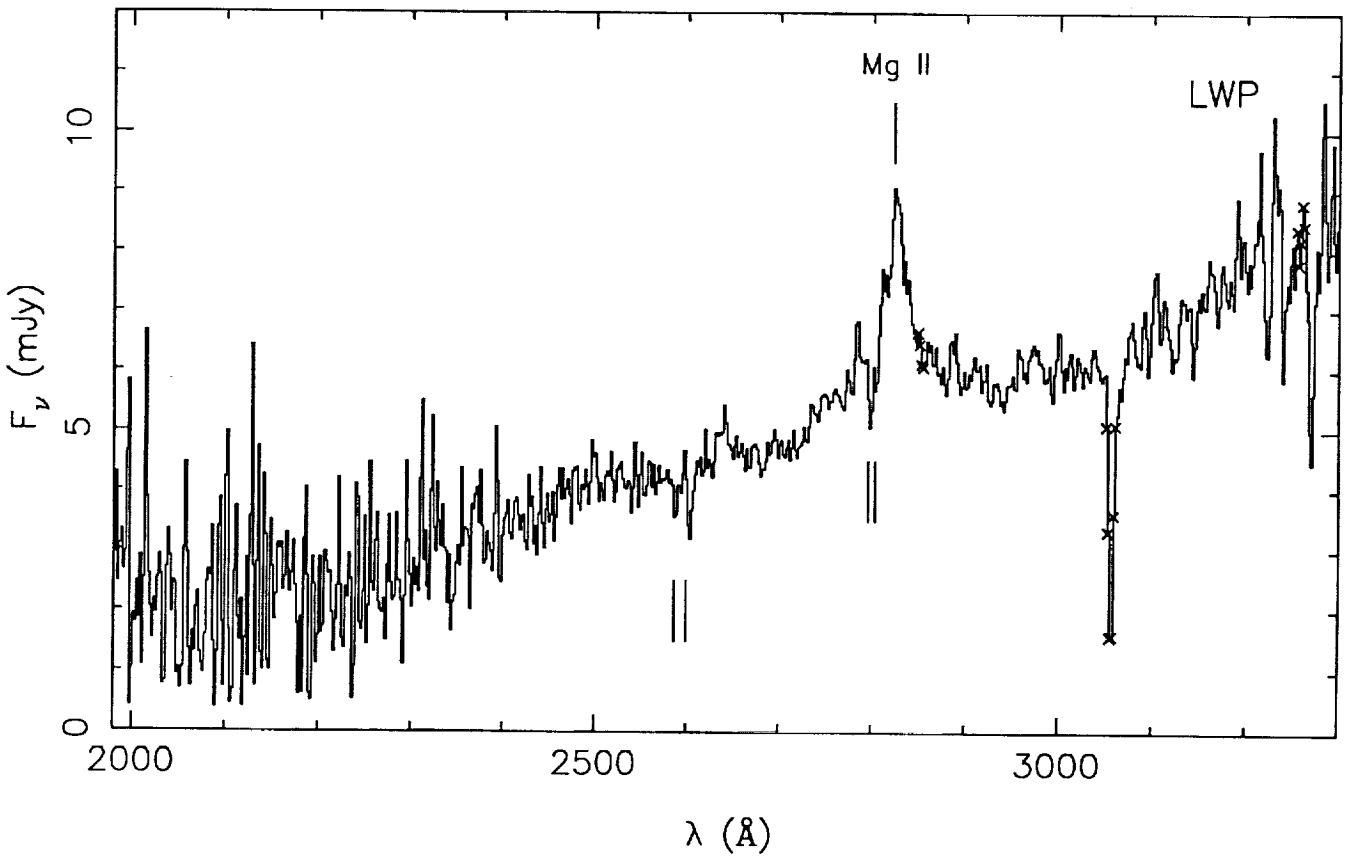
Mg II
LWP
F$_\nu$ (mJy)
λ (Å)
0
5
10
2000
2500
3000

Figure 2

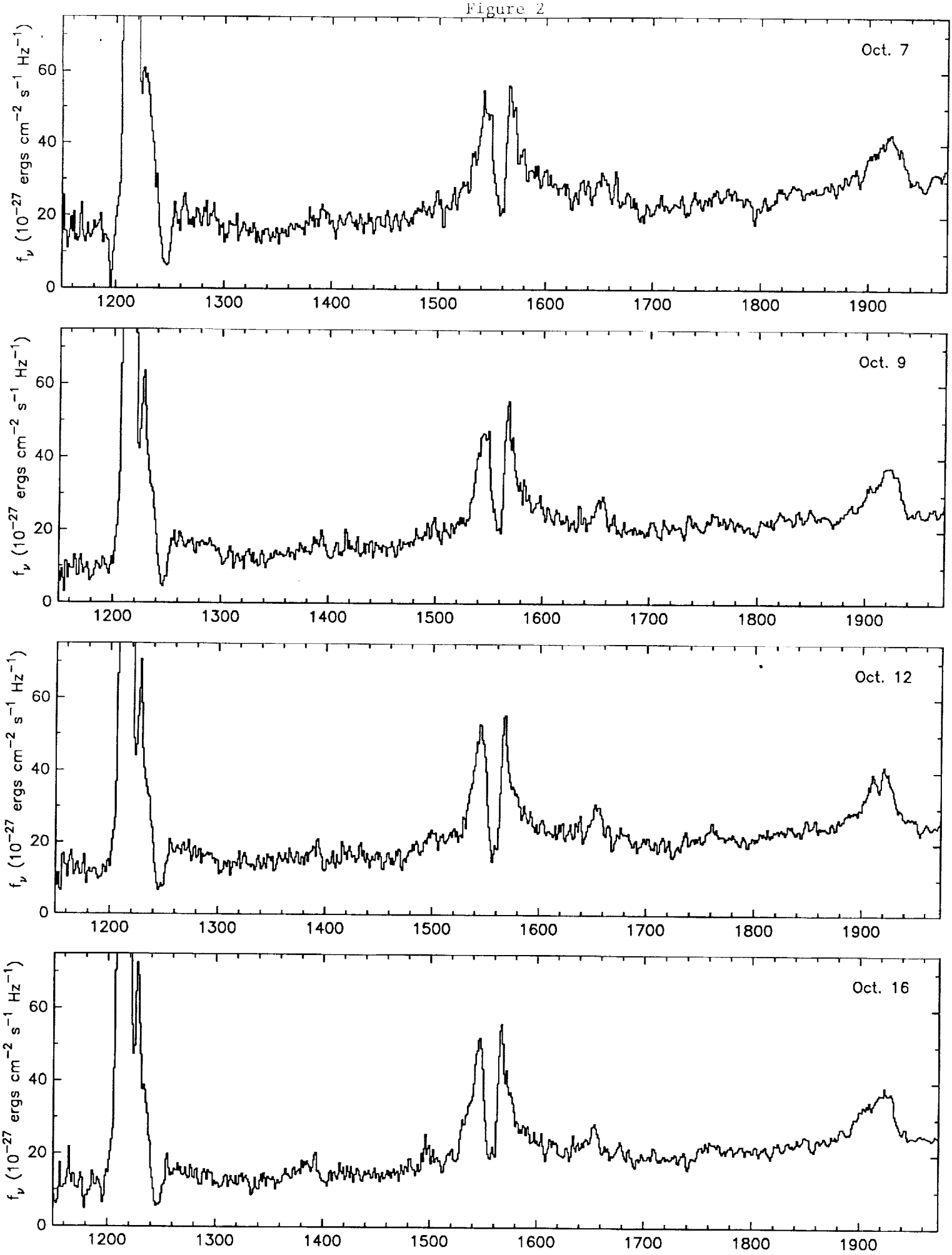
Oct. 7
Oct. 9
Oct. 12
Oct. 16
f_ν (10^{-27} ergs cm^{-2} s^{-1} Hz^{-1})
0
20
40
60
1200
1300
1400
1500
1600
1700
1800
1900

Figure 3a

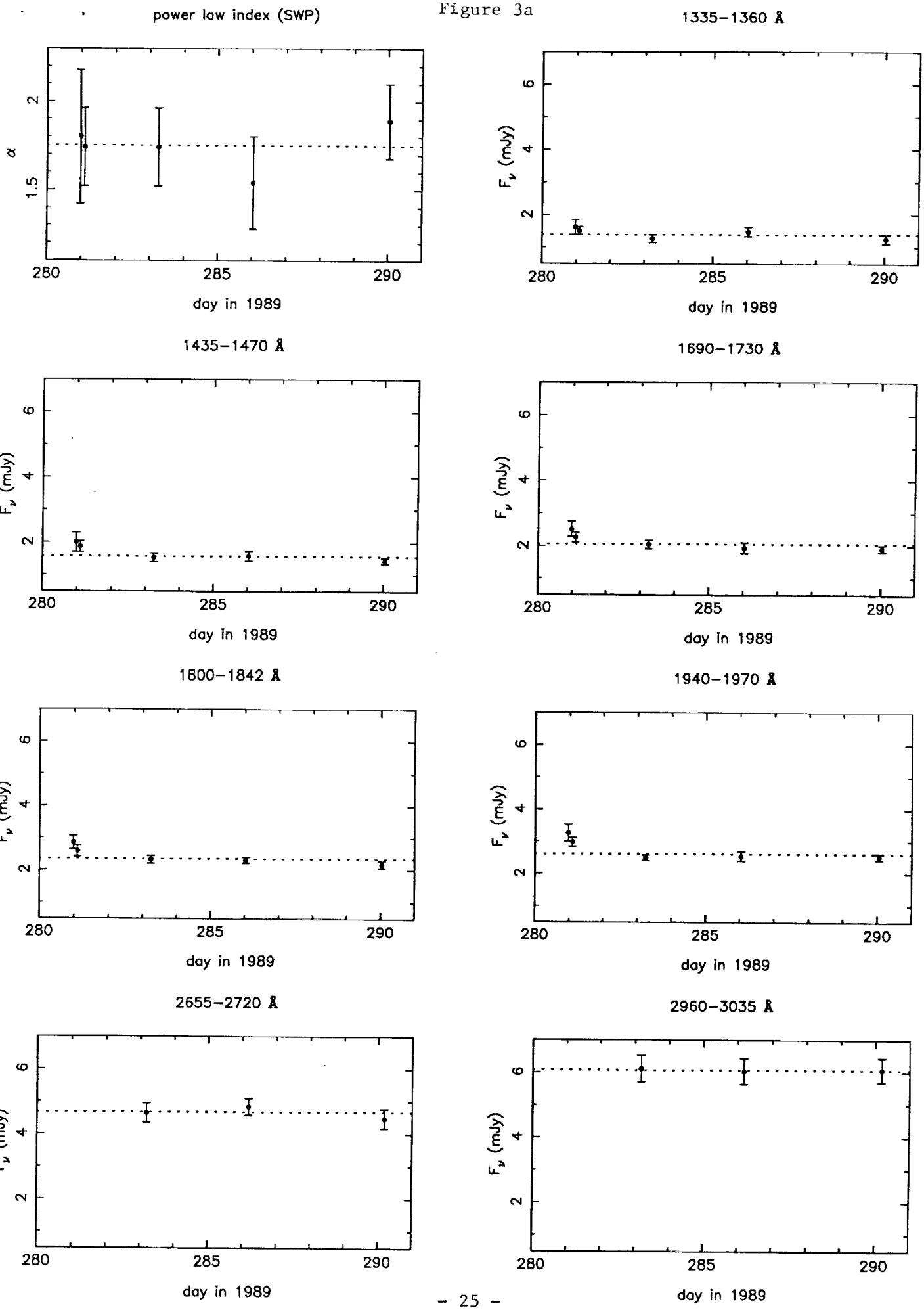
power law index (SWP)
α
day in 1989
1335–1360 Å
1435–1470 Å
1690–1730 Å
1800–1842 Å
1940–1970 Å
2655–2720 Å
2960–3035 Å
F_ν (mJy)

Figure 3b

power law index (SWP+LWP)

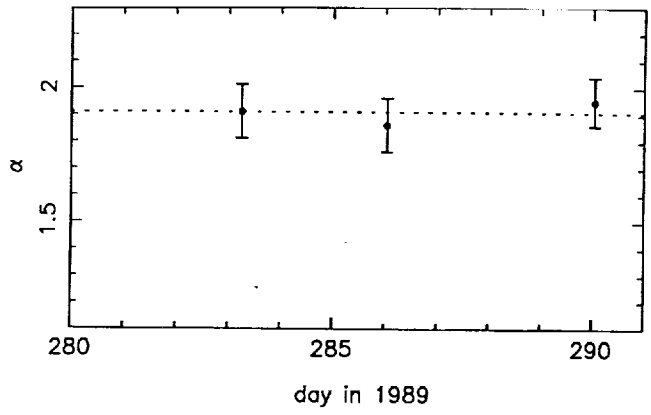

1335–1360 Å

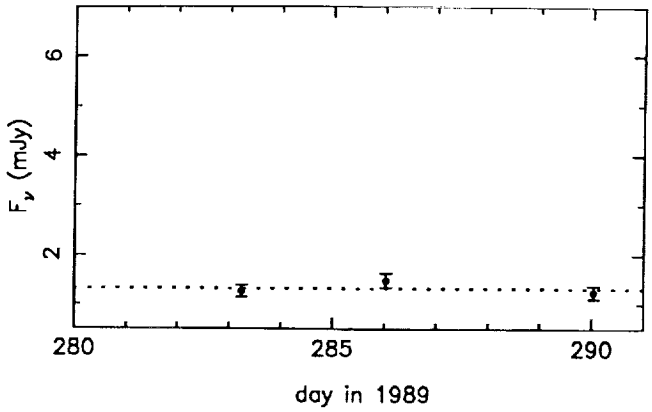

1435–1470 Å

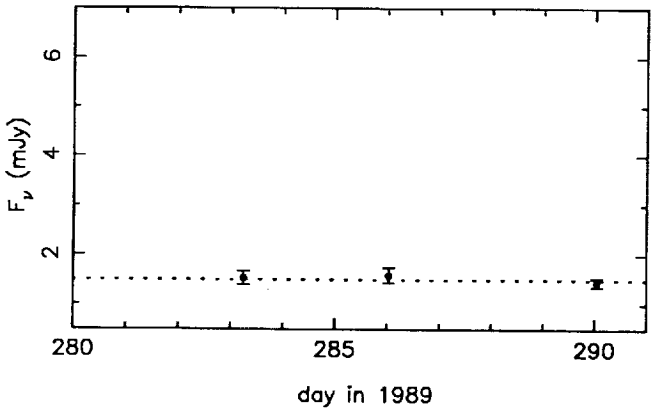

1690–1730 Å

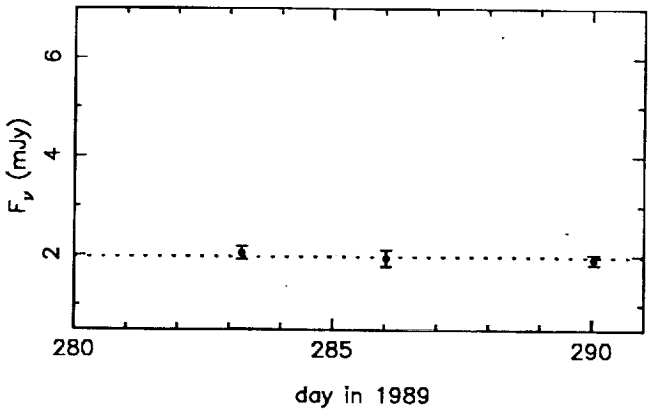

1800–1842 Å

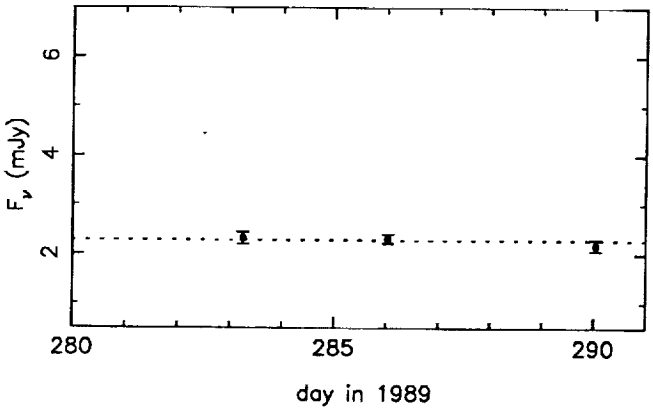

1940–1970 Å

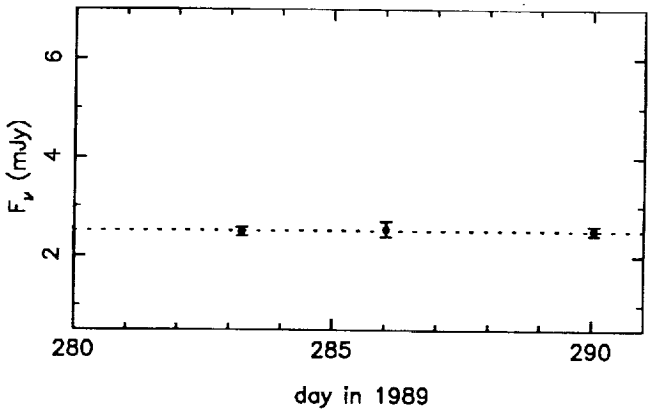

2655–2720 Å

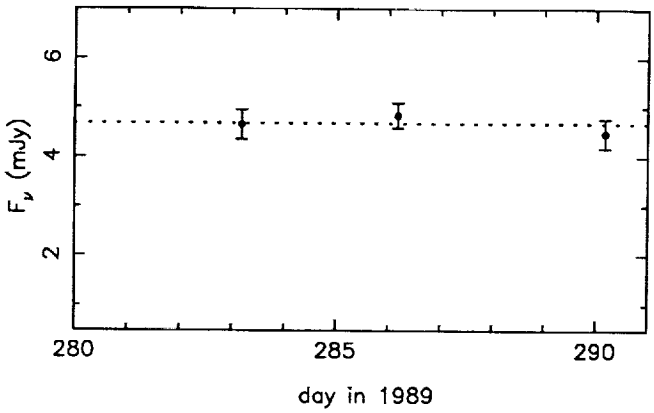

2960–3035 Å

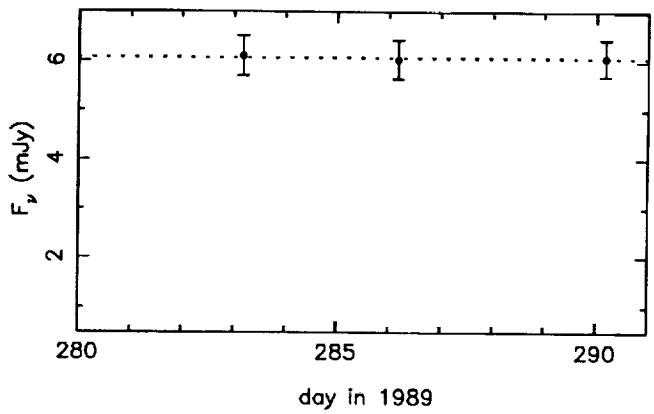

APPENDIX

Papers Published Under NASA Grant NAG 5-1140

"The Ultraviolet Spectrum and Continuum Energy Distribution of the Bright Quasar H1821+643," M. Kolman, J. P. Halpern, C. R. Shrader, and A. V. Filippenko, *Ap. J.*, **373**, 57 (1991).

THE ASTROPHYSICAL JOURNAL, 373:57–65, 1991 May 20

THE ULTRAVIOLET SPECTRUM AND CONTINUUM ENERGY DISTRIBUTION OF THE BRIGHT QUASAR H1821+643

MICHIEL KOLMAN & JULES P. HALPERN[1]
Columbia Astrophysics Laboratory, Columbia University, 538 West 120th Street, New York, NY 10027
CHRIS R. SHRADER[2]
Astronomy Programs, Computer Sciences Corporation
AND
ALEXEI V. FILIPPENKO[1,3]
Astronomy Department, University of California, Berkeley, CA 94720
Received 1990 August 20; accepted 1990 November 9

ABSTRACT

We report on the first UV observations of the bright QSO H1821+643. With $V = 14.2$ mag and $z = 0.297$, H1821+643 is the second brightest object in the sky at $z > 0.1$. The *IUE* data are combined with new optical spectroscopy, and existing infrared and X-ray data, to reveal a strong optical/UV "big bump," which continues past the Lyman limit in the rest frame of the QSO. A possible turnover at the high-frequency side of the UV continuum constrains fits of a thin accretion disk model to a large black hole mass ($M \simeq 3 \times 10^9\ M_\odot$) and high accretion rate ($\dot{M} \simeq 19\ M_\odot\ \mathrm{yr}^{-1}$), but a small disk size ($R_{\rm out}/R_{\rm in} \simeq 12$). The shape of the UV continuum was found to be variable, with a hardening of the spectrum when the source was brighter. Because of its location only 3° from the ecliptic pole, H1821+643 will be an important object for simultaneous UV and soft X-ray monitoring to test for a common origin of the UV bump and soft X-ray excess.

Subject headings: quasars — spectrophotometry — ultraviolet: spectra

1. INTRODUCTION

Twenty years after the discovery of QSOs, one of the brightest objects of this class had yet to be noticed. Known as H1821+643, it was identified by Pravdo & Marshall (1984) as the counterpart of an X-ray source first detected by *HEAO 1* and then by *Einstein*. With $V = 14.2$ mag, it is the brightest object after 3C 273 at $z > 0.1$. The brighter members of a class often contribute disproportionately to our knowledge of their physics, because they can be studied well at many wavelengths. The intermediate redshift of H1821+643 ($z = 0.297$) makes it well-suited to a study of the intrinsic ultraviolet continuum, as higher redshift objects suffer from absorption by intergalactic H I clouds. Moreover, its location only 3° from the ecliptic pole [the position is $\alpha(1950) = 18^{\rm h}21^{\rm m}41\overset{\rm s}{.}67$, $\delta(1950) = 64°19'0\overset{''}{.}8$] makes H1821+643 an important object for monitoring programs done with satellites. In particular, it is an ideal object to test for a common origin of the UV big bump and the soft X-ray excess, an association which has yet to be proven.

In this paper, we report new ultraviolet and optical spectrophotometry which we combine with existing infrared and X-ray data to study the continuum energy distribution of this QSO. The combined optical and *IUE* spectra show a strong UV bump. The moderate redshift allows the detection of flux past the Lyman limit in the rest frame, while allowing for optimal coverage of the UV bump within the *IUE* bandpass. We present fits to a thin disk model, which require large mass and accretion rate for this high luminosity QSO, but also indicate a small outer radius for the disk.

The strong soft X-ray excess, which was attributed to H1821+643 in the *HEAO A-2* data of 1977, is absent in all subsequent X-ray observations, which resemble the "canonical" hard power law. Although we take this variable soft excess at face value for the purpose of this paper, we also discuss other soft X-ray sources in the vicinity of the QSO which could have confused the *HEAO A-2* low-energy detector.

2. OBSERVATIONS

2.1. *The X-Ray Identification*

When H1821+643 was identified by the *Einstein* imaging proportional counter (IPC), comparison with *HEAO A-2* data obtained 3 yr earlier indicated that a factor of 4 decrease in the soft X-ray flux had occurred between 1977 and 1980 (Pravdo & Marshall 1984). The change could be described as the disappearance of the soft X-ray excess, which is clearly present in the *HEAO A-2* low energy detector (LED), and not evident in the *Einstein* IPC. Subsequent observations by *EXOSAT* in 1984 and 1985 (Warwick, Barstow, & Yaqoob 1989) also did not detect a soft X-ray excess, leading these authors to consider the possibility that the *HEAO A-2* LED detector had been confused by another soft X-ray source in the field, possibly the central star of the planetary nebula K1-16 (Grauer & Bond 1984) which is 100″ from the QSO. But having estimated the flux from K1-16 in the 0.2–2 keV bandpass of the LED, Warwick et al. (1989) concluded that it could not have contributed significantly to the observed soft X-ray excess.

We can further address this issue with the *Einstein* IPC data since the IPC bandpass includes that of the *HEAO A-2* LED. Moreover, the IPC data were taken as part of a survey of the north ecliptic pole region, which can be searched for other soft X-ray sources in the vicinity of the LED error box. There were four overlapping fields, all of which included H1821+643, although in three of these the QSO fell just outside the support ribs of the detector, hampering detailed quantitative analysis.

[1] Guest Observer with the *International Ultraviolet Explorer* Satellite.
[2] Staff member, *IUE* Observatory, NASA/GSFC. Postal address: Code 668.1, NASA/GSFC, Greenbelt, MD 20771.
[3] Presidential Young Investigator.

The X-ray position and pointlike nature of the source in the IPC map are consistent with identification with the QSO and not the planetary nebula, although it cannot be excluded that K1-16 might make a small contribution to the IPC X-ray source. More worrisome for the interpretation of the soft excess in the LED is another X-ray source 36′ to the northeast of the QSO, which is of comparable intensity. We identified this source with the 8.0 mag K0 star, SAO 17878. The error boxes of the several *HEAO-1* detectors, in addition to the optical positions of possible confusing sources, are shown in Figure 1. The X-ray flux of SAO 17878 in the 0.1–3.5 keV band as observed with the IPC is 9×10^{-12} ergs cm^{-2} s^{-1}, about half that of the QSO at the time of the *Einstein* observations. In the absence of detailed knowledge about its variability, it cannot be ruled out that this star contaminated the LED error box (Nugent et al. 1983), on whose edge it lies. However, the X-ray flux from this star would have to have been at least 4 times larger than the *Einstein* value for it to have made a substantial contribution to the LED flux. The only other X-ray source close to the LED error box is a 5.0 mag F5 star, SAO 17828, with an IPC flux of about 1×10^{-12} ergs cm^{-2} s^{-1}. This source is an even less likely contributor. In summary, we can be certain that the hard X-rays arose in the QSO, as indicated by the IPC source and the small *HEAO A-1* error box of 0.05 deg^2 (Wood et al. 1984). We can also be certain that the soft excess was *not* present during the *Einstein* or *EXOSAT* observations. Whether the soft excess observed by the *HEAO A-2* LED arose exclusively in the QSO cannot be determined, although this appears highly likely.

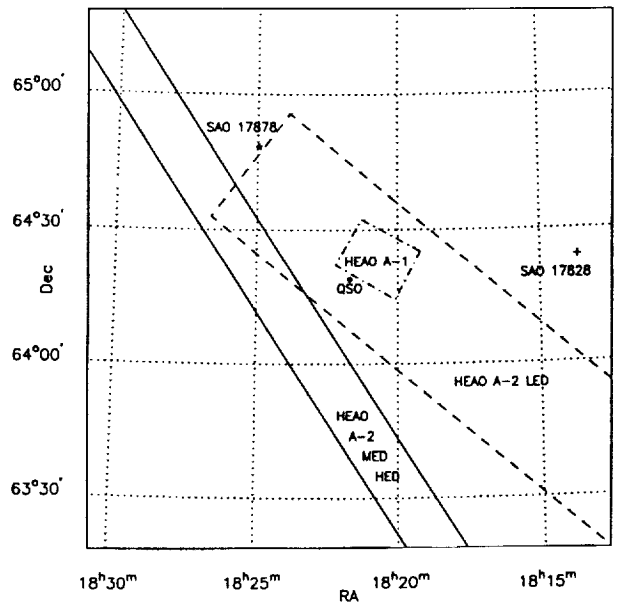

FIG. 1.—Error boxes of the *HEAO* observations around H1821+643 (indicated by the filled circle labeled QSO). The *HEAO A-2* MED-HED error box (Marshall et al. 1979) is indicated by the solid lines; the *HEAO A-2* LED error box (Nugent et al. 1983) is indicated by the dashed lines; the *HEAO A-1* error box (Wood et al. 1984) is indicated by the dot-dashed lines. The star indicates the position of SAO 17878, which could contribute some of the detected flux in the *HEAO A-2* LED band. The plus sign indicates the position of the weak IPC source SAO 17828. The IPC error circles for the QSO and SAO stars have a typical diameter of 1′ and are too small to be drawn in this figure. All positions are in 1950 coordinates.

TABLE 1

EINSTEIN IPC SPECTRUM OF H1821+643

Date	1980 May 25
Exposure time (s)	960.0
IPC counts s^{-1} (0.1–3.9 keV)	0.508 ± 0.023
F_X (0.1–3.5 keV)[a]	1.74×10^{-11}
L_X (0.1–3.5 keV)[b]	9.6×10^{45}
A[c]	4.23×10^{-3}
α (68% confidence)	0.60 ± 0.34
(90% confidence)	$(+0.62, -0.45)$
N_H (cm^{-2}) (68% confidence)	$2.0\ (+1.8, -1.5) \times 10^{20}$
(90% confidence)	$< 5.0 \times 10^{20}$
χ^2_{min} (per d.o.f.)	1.34

[a] Flux (ergs cm^{-2} s^{-1}) in observed energy band.
[b] Luminosity (ergs s^{-1}) in intrinsic energy band, corrected for absorption and assuming $\alpha = 0.6$, $H_0 = 50$ km s^{-1} Mpc^{-1}, and $q_0 = 0$.
[c] Normalization constant.

2.2. *The X-Ray Spectrum*

We performed a standard spectral analysis on the single *Einstein* IPC observation in which the QSO fell inside the support ribs. The results are listed in Table 1. Power-law fits yielded a best-fit energy index $\alpha = 0.6$, with 68% confidence limits of 0.26–0.94, and 90% confidence limits of 0.15–1.12. The 90% upper limit on the column density N_H is 5×10^{20} cm^{-2}, which is consistent with the 21 cm value of 4.1×10^{20} cm^{-2} (Stark et al. 1990). Hard X-ray spectral measurements by *EXOSAT* (Warwick et al. 1989) and *Ginga* (Turner et al. 1989; Kii et al. 1991) are consistent with an extrapolation of the IPC data, both in spectral index and normalization. Therefore, it seems likely that the soft excess observed by the *HEAO A-2* LED is a separate component, which varies independently of the hard power law.

2.3. *The Ultraviolet Observations*

In 1987 we obtained the first UV spectra of H1821+643 with the *IUE* satellite. The strong and broad Lyman-α emission line was saturated in the 300 minute exposure of the SWP. A subsequent shorter exposure (120 minutes) resulted in optimal detection in the Lyman-α line. All the *IUE* observations are listed in Table 2. The images were obtained with the large aperture in the low-dispersion mode, resulting in a spectral resolution of about 5 Å and about 8 Å for the SWP and LWP, respectively.

The spectra were obtained from the line-by-line images with the Gaussian extraction routines at the Goddard Regional Data Analysis Facility to minimize the noise while maintaining accurate flux levels. We corrected the spectra for the effects of interstellar reddening, using the extinction curve of Seaton (1979) and $E(B-V) = 0.085$ mag. The color excess is based on

TABLE 2

IUE OBSERVATIONS OF H1821+643

Image	Int. time (minutes)	Date
SWP 31431	300	1987 Jul 29
LWP 11294	130	1987 Jul 29
SWP 31523	120	1987 Aug 10
SWP 35516	275	1989 Feb 9
LWP 14996	95	1989 Feb 9
SWP 36396	300	1989 Jun 4
LWP 15659	120	1989 Jun 4

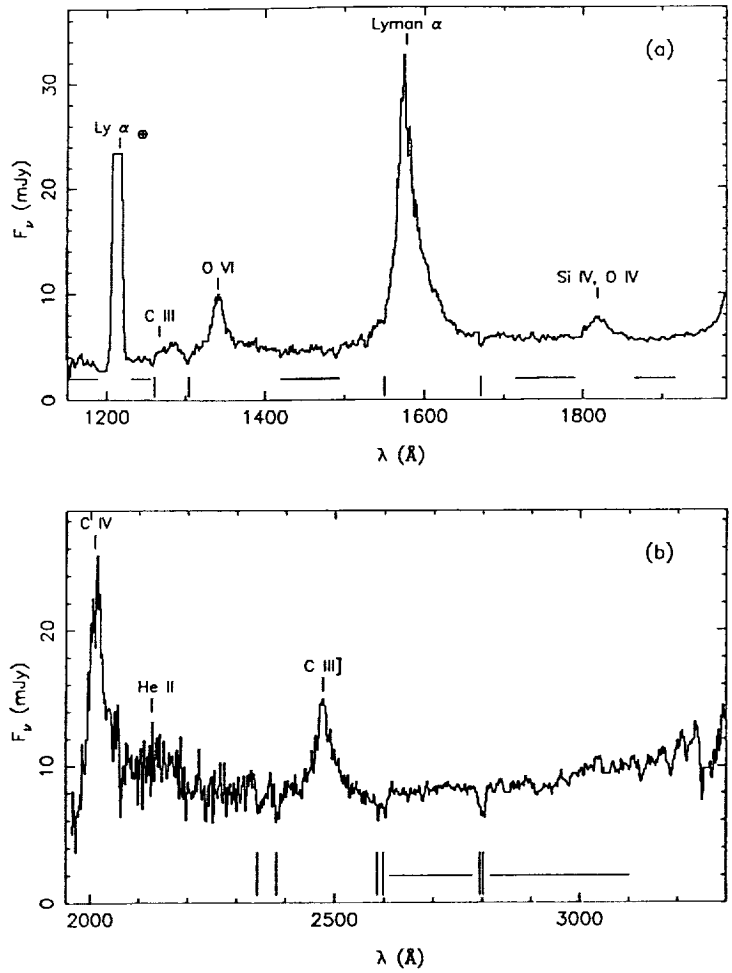

FIG. 2.—(*a*) Co-added SWP spectrum of H1821+643 obtained with *IUE*, corrected for the estimated interstellar extinction of $E(B-V) = 0.085$ mag. The Lyman-α emission is patched in from the unsaturated image, SWP 31523. (*b*) LWP spectrum. The horizontal lines denote the wavelengths selected as the continuum and used in Figs. 4 and 6. The vertical tick marks indicate the detected interstellar absorption lines.

the neutral hydrogen column density in the direction of H1821+643 ($N_H = 4.1 \times 10^{20}$ cm^{-2}, Stark et al. 1990) and the $N_H/E(B-V)$ ratio of 4.8×10^{21} cm^{-2} mag^{-1} (Bohlin, Savage, & Drake 1978). We did not correct for any internal reddening, as there is now growing evidence that the intrinsic extinction in QSOs is very small (Sun & Malkan 1989a, and references therein). We deleted the data points which were flagged because of the presence of a reseau. The co-added spectrum is shown in Figure 2. The overall continuum level decreases slightly with increasing frequency. The flux level is sensitive to the correction for interstellar extinction, but even if the spectrum is overcorrected for reddening [up to $E(B-V) = 0.2$ mag], a downward trend with shorter wavelengths remains. Despite the decline in sensitivity below 1200 Å, there is strong emission shortward of the Lyman limit, which is redshifted to 1182 Å (Fig. 3).

As listed in Table 2, there are three series of observations with *IUE*, each resulting in at least one SWP and LWP image: the first in 1987, the second in 1989 February, and the third in 1989 June. Two SWP spectra were obtained in 1987: a long exposure with optimal detection of the continuum level and a short exposure with optimal detection of the Lyman-α emission line. In order to study the continuum, the spectra were binned into about 10 data points per camera, avoiding the major emission lines and the Galactic absorption lines. If we compare these three series of observations, no significant changes could be found between the first and second series, while the spectral shape did change significantly between the second and third series. As shown in Figure 4, the emission between 2000 and 3000 Å decreased in intensity, while the short wavelength side increased by about 10%, resulting in a hardening of the spectrum between 1989 February and June.

2.4. *Optical Spectroscopy*

Optical CCD spectra of H1821+643 covering the wavelength range 3138–10046 Å were obtained on 1988 October 3 UT using four different grating settings of the UV Schmidt spectrograph (Miller & Stone 1987) at the Cassegrain focus of the Shane 3 m reflector at Lick Observatory. The spectra were obtained through a long slit of width 8″, oriented along the parallactic angle (Filippenko 1982). The airmass was 1.3, conditions were photometric, and the seeing was about 1″. Typical integration times per setting were 300–500 s. The spectral resolution was 5–8 Å below about 7200 Å, and 10–16 Å in the near-IR region.

Standard techniques were used to extract one-dimensional spectra from the CCD data. These included subtraction of the bias level, division by a flat field, removal of cosmic rays, cor-

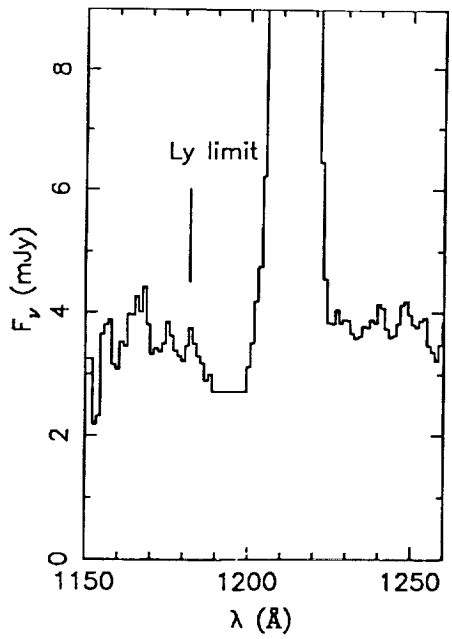

FIG. 3.—Expanded view of Fig. 2*a* shows the presence of substantial flux below the Lyman limit at 1182 Å (indicated by the vertical tick-mark). We estimate that the covering fraction at the Lyman limit must be less than 0.09. The strong emission line around 1216 Å is geocoronal Lyman-α. The data points around 1190 Å are deleted because of the presence of reseau.

rection for geometric distortion and misalignments, and subtraction of the background sky. Several stars from the lists of Oke & Gunn (1983) and Massey et al. (1988) were used to flux calibrate the spectra, as well as to remove telluric absorption bands at wavelengths longer than 6200 Å. Excellent agreement in absolute fluxes and spectral shapes was found in overlapping spectral regions. However, the wavelength scale is uncertain by about 4 Å, since the observations were obtained through a wide slit. The redshift derived from the [O III] lines is 0.2972 ± 0.0006.

The overall optical spectrum of H1821+643, corrected for extinction [$E(B-V) = 0.085$ mag], is shown in Figure 5. The near-UV flux joins that of the *IUE* spectrum very well, as can been seen by comparison of Figures 2 and 5.

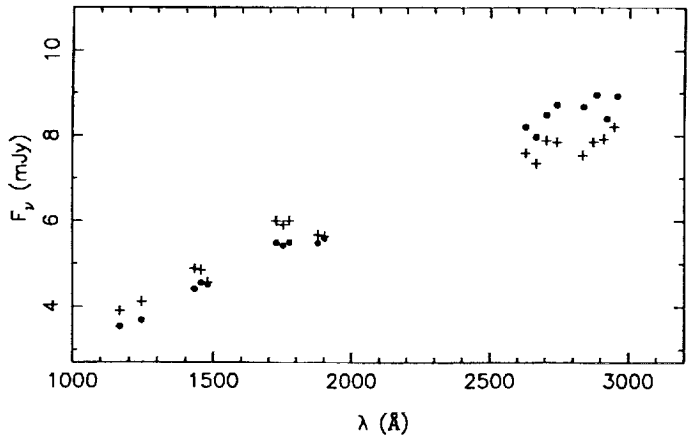

FIG. 4.—Change in the UV continuum shape between 1989 February 9 (indicated by filled circles) and 1989 June 4 (indicated by plus signs). The flux increased by about 10% at the shortest wavelengths while the flux decreased at the long-wavelength side, corresponding to a hardening of the spectrum.

2.5. *Optical and Infrared Photometry*

The *UBV* photometry was obtained by S. Vrtilek with the 0.9 m telescope at Kitt Peak National Observatory on 5 nights centered around 1988 October 10. Variability in the *V* band was less than 0.03 mag from night to night, and less than 0.04 mag and 0.2 mag for $B-V$ and $U-B$, respectively. The average magnitudes are listed in Table 3. Near infrared magnitudes from the Infrared Telescope Facility (IRTF) in the *J* (1.25 μm), *H* (1.65 μm), *K* (2.2 μm), and *L'* (3.8 μm) bands were provided by M. Elvis, and are listed in Table 3. In the far infrared, *IRAS* detections in all four bands were published by Neugebauer et al. (1986), and are also listed in Table 3.

The overall continuum distribution derived from all the above data and shifted to the rest-frame is shown in Figure 6. Throughout this article λ and ν denote observed wavelength and frequency, while λ_0 and ν_0 denote the wavelength and frequency in the rest-frame of the QSO.

2.6. *Radio Observations*

VLA observations at 6 cm with a partial array of six dishes and an exposure time of 20 minutes yielded an upper limit of 15 mJy, establishing this QSO as radio quiet.

3. RESULTS

3.1. *Emission Shortward of the Lyman limit*

The redshift of H1821+643 (0.297) is high enough to shift the Lyman limit to 1182 Å, into the wavelength range of *IUE*, but low enough to avoid absorption by intervening H I clouds. Substantial flux is detected below 1182 Å in all our SWP spectra (Fig. 2). An upper limit to the covered fraction of the continuum source as derived from the flux levels below and above 1182 Å is estimated at 0.09; a small value consistent with the absence of X-ray absorption in this and other bright AGNs. This small covering fraction of less than 0.1 is also expected in a high luminosity QSO such as H1821+643 on the basis of photon counting arguments concerning the photoionization of clouds on the BLR. Rest-frame Lyman continuum absorption has been reported (Kinney et al. 1985) in less than 10% of all AGNs. Another bright QSO, 3C273, is a possible

TABLE 3

PHOTOMETRY OF H1821+643

Band	Magnitude	Flux (mJy)
U[a]	13.30	9.04
B[a]	14.30	8.12
V[a]	14.26	7.55
J[b]	13.09	8.8
H[b]	12.19	13.0
K[b]	11.12	22.1
L'[b]	8.95	60.5
12 μm[c]		236
25 μm[c]		373
60 μm[c]		953
100 μm[c]		2164
6 cm		<15

[a] Magnitude averaged over 5 nights, obtained with the automated filter photometer on the 0.9 m telescope at Kitt Peak National Observatory around 1988 October 10 (S. Vrtilek 1988, private communication).

[b] IRTF instrumental magnitude, obtained with 6" diameter aperture and the InSb detector (RC2) on 1988 April 25 (M. Elvis 1988, private communication).

[c] *IRAS* fluxes (Neugebauer et al. 1986).

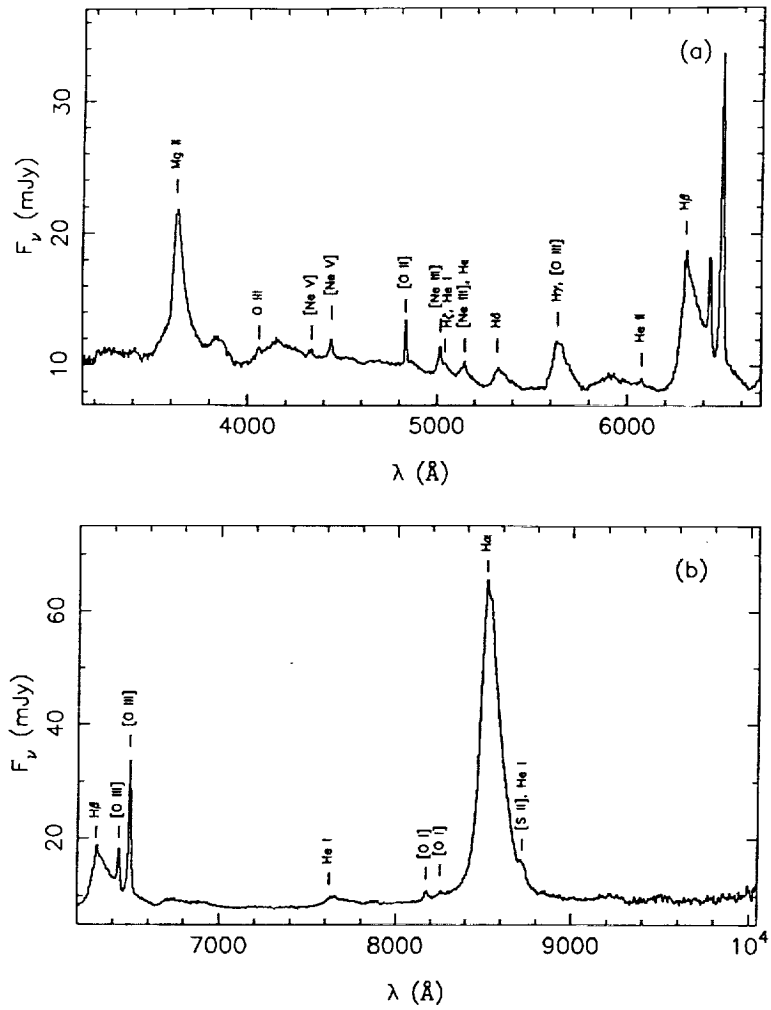

FIG. 5.—Optical spectrum of H1821+643 obtained at Lick Observatory on 1988 October 3 under photometric conditions. The interstellar extinction correction for $E(B-V) = 0.085$ mag has been applied. The continuum appears bumpy due to the contribution of blended Fe II lines (e.g., around 3800, 4200, 5900, and 6700 Å).

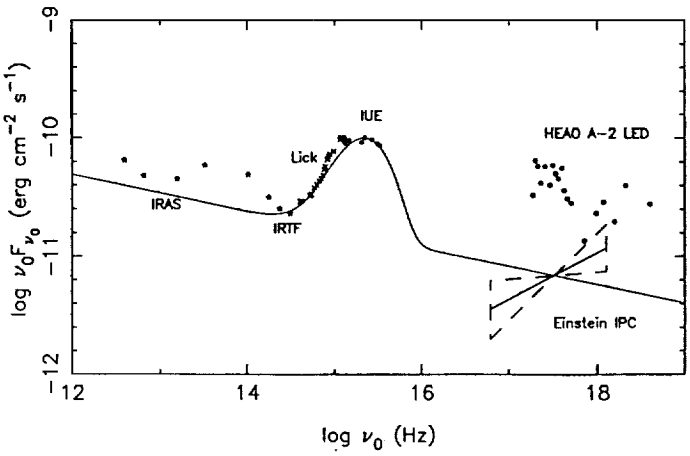

FIG. 6.—Overall continuum spectrum of H1821+643 plotted in the QSO rest frame, with the co-added *IUE* data from 1987. Note the turnover of the UV bump and the large amplitude variation between the X-ray observations. The power-law plus thin accretion disk (*solid line*) fit with $M = 3 \times 10^9\ M_\odot$, $\dot{M} = 19\ M_\odot\ \mathrm{yr}^{-1}$, and $R_{out}/R_{in} = 12$, deviates between $\log \nu_0 = 14.8$ and $\log \nu_0 = 15.2$ due to the Balmer continuum and Fe II line emission.

exception, as a Lyman discontinuity has been reported in combined *IUE/Voyager* data (Reichert et al. 1988). By contrast, the continuum spectrum of H1821+643 seems to turn over smoothly well longward of the Lyman limit, which argues that the thermal peak, rather than any Lyman limit absorption, is responsible for the drop in flux level at the high-frequency side of the *IUE* spectrum. However, one must be aware of the possibility that Lyman continuum absorption is an intrinsic property of accretion disks in AGNs (Sun & Malkan 1987; Sun & Malkan 1989b; Scott & O'Dell 1989), and that a suitable smearing of the Lyman edge due to strong Doppler and gravitational effects in the inner disk might cause some of the turnover which is observed.

3.2. *Continuum Energy Distribution*

None of the observations in different wavebands were simultaneous; nevertheless, the infrared through UV data are very continuous. There is a steep rise in the flux level at optical frequencies, and the *IUE* data points indicate a strong UV bump. The prominence of the UV bump is similar to the one detected in the optical/UV bump prototype PG 1211+143, but it could be observed to higher rest-frame frequencies due to the higher redshift ($z = 0.297$ vs. $z = 0.085$ for PG 1211+143).

In all the spectra except the one obtained in 1989 June, there is evidence for a turnover at the high-frequency side (around $\log \nu_0 = 15.3$).

Because of the 5 μm feature displayed by the IR data points, the power law, if any, is not well defined in the infrared. By forcing a fit to the 60 μm and 1 μm data points, we find $\alpha = 1.16$ (where $F_\nu \propto \nu^{-\alpha}$). Because there is a strong correlation between the IR and hard X-rays in QSOs (Edelson & Malkan 1986; Kriss 1988), a single power law might be extrapolated from $\log \nu_0 \approx 12$ to $\log \nu_0 \approx 18$. The turn-up from the overall power law of the hard X-ray data (both for the *Einstein* data and the 2–10 keV *HEAO 1* data) is typical for the high-frequency side of the continuum energy distribution in QSOs (Elvis 1988). Considering the large amplitude of variability in the X-rays, it is impossible to estimate the soft X-ray flux level at the time of the *IUE* observations, which would be important for models of the soft X-ray excess.

3.3. *Emission Lines*

Information on continuum emission in the unobservable EUV gap can be derived from the UV and optical emission lines, which are powered by photons with EUV energies. To this end, we measured the major emission lines in the UV and optical spectra. No significant differences in line fluxes were found from one *IUE* observation to the other; therefore, all the *IUE* spectra were coadded and dereddened. The measured line properties are listed in Table 4 and the lines are identified in Figures 2 and 5. The Lyman-α emission line could only be measured in SWP 31523, as the other SWP spectra were saturated at this line. The major source of error in the line measurements is the uncertainty in the continuum level, which is contaminated by the broad wings of the emission lines, Galactic absorption lines, and blended Fe II line and Balmer continuum emission. For the O VI λ1034 emission line only the narrow component was measured (with a full width at zero intensity, FW0I, of about 40 Å), as it was unclear to where the broad wings extend (possibly from 1280 to 1380 Å, encompassing the Galactic absorption feature around 1300 Å). This uncertainty around the O VI line also complicated the measurement of the upper limit to C III λ977 at its redshifted wavelength of 1267 Å, as well as the measurement of the O I λ1302, Si II λ1304 absorption feature.

TABLE 4

EMISSION-LINE MEASUREMENTS OF H1821+643

ID[a]	Intensity[b]	Flux[c]	EW[d] (Å)
C III λ977	<35.0	<20.3	<5.0
O VI λ1034[e]	137.1	83.4	16.8
Lyα λ1216, (N V λ1240)	963.5	626.9	156.0
Si IV λ1397, O IV λ1407	49.8	32.8	10.0
C IV λ1549	504.8	305.9	111.4
He II λ1640, (O III] λ1663)	161.9	91.7	36.8
C III] λ1909	115.2	78.1	30.4
Mg II λ2798	222.6	186.5	98.7
O III λ3133	1.8	1.6	1.0
[Ne V] λ3345	2.1	1.8	1.3
[Ne V] λ3426	4.3	3.8	2.8
[O II] λ3727	5.1	4.6	4.1
[Ne III] λ3869	4.5	4.2	4.7
Hζ λ3889, He I λ3888	2.4	2.2	2.5
[Ne III] λ3968, Hϵ λ3970	3.6	3.3	3.6
Hδ λ4102	11.0	10.3	13.2
Hγ λ4340, [O III] λ4363	29.0	27.8	39.3
He II λ4686	0.6	0.6	1.0
Hβ λ4861	100.0	100.0	172.6
[O III] λ4959	8.4	8.3	10.4
[O III] λ5007	28.6	28.4	40.3
He I λ5876	9.8	10.2	24.0
[O I] λ6300	1.6	1.7	4.0
[O I] λ6363, ([Fe X] λ6375)	0.9	0.9	2.0
Hα λ6563, ([N II] $\lambda\lambda$6548,83)	333.3	352.3	895.1
[S II] λ6716,30 (He I λ6678)	4.8	5.1	9.9

[a] Identification of emission line and rest wavelength; the lines in parentheses denote only minor contributions.

[b] Intensity corrected for Galactic reddening, relative to Hβ, with $I(\mathrm{H}\beta) = 1.05 \times 10^{-12}$ ergs cm^{-2} s^{-1}.

[c] Observed flux relative to Hβ with $F(\mathrm{H}\beta) = 8.63 \times 10^{-13}$ ergs cm^{-2} s^{-1}.

[d] Observed equivalent width.

[e] Narrow component only (FW0I $\sim$40 Å).

These UV observations are the first to be conducted for H1821+643. There were, however, previous optical observations with emission line measurements from 1981 (Pravdo & Marshall 1984). The equivalent widths listed by these authors for Mg II, Hγ and Hβ are smaller (by about 30%) than our measurements, and larger (by 15%) for [O III] λ5007. Compared to a sample of 20 intermediate redshift QSOs ($z < 0.84$, Kinney et al. 1985) the EW of Lyman-α for H1821+643 is typical, being close to the sample's average. Kwan & Krolik (1981) compiled the average and range of permitted line ratios for a large sample of QSOs. No single line ratio observed in H1821+643 is outside this sample's range. Compared to the mean, the observed ratios of Lyα/Hβ, C IV λ1549/Lyα, and Mg II λ2798/Hβ in H1821+643 are large (by a factor of about 1.5), while the C III] λ1909/C IV λ1549 ratio is half the mean value.

Considering the overall energy distribution of H1821+643, it would be of interest to determine where the spectrum peaks: at *IUE* frequencies as suggested by the detected turnover, at soft X-ray energies as indicated by the *HEAO 1* data, or in the unobservable EUV gap. Krolik & Kallman (1988) investigated this question theoretically by modeling the effects of the several different accretion disk spectra [i.e., bare power law, power law plus disk spectrum peaking at 10 eV ($\log \nu_0 \sim 15.4$), and one peaking at 80 eV ($\log \nu_0 \sim 16.3$)] on the emission line formation. Although the ionization parameter Ξ is far more important than the shape of the ionizing spectrum in determining the line emission, there are line ratios which are relatively insensitive to the ionization parameter.

The observed line ratios in H1821+643 are consistent with a power law plus disk spectrum peaking at 10 eV, i.e., in the UV, within the context of the Krolik & Kallman (1988) model. All ratios are within the model range (with the pressure as a free parameter between 6.3×10^{13} and 20×10^{13} K cm^{-3}) for the high ionization case ($\Xi = 2.0$), except for C III] λ1909/C IV λ1549 (the one ratio that is substantially smaller than the average value for Kwan & Krolik's 1981 sample of AGNs). A high Ξ might be expected for an ionizing spectrum peaking at low energies in order to produce enough high-ionization species.

3.4. *Absorption Lines*

The location of H1821+643 at $(l, b) = (94°, 27°)$ and the moderate column density of 4.1×10^{20} cm^{-2} are ideal for study of interstellar absorption. The Galactic longitude of H1821+643 permits optimal velocity separation of distant matter from local matter, while the low-latitude permits the viewing of distant matter at large height above the Galactic plane. Therefore, future high-resolution studies of the absorp-

TABLE 5

ABSORPTION-LINE MEASUREMENTS OF H1821+643

ID	EW (Å)
S II λ1251, 1254, 1260, Si II λ1260	0.8
O I λ1302, Si II λ1304	2.6
C IV λ1548,51	<0.7
Al II λ1671	0.6
Fe II λ2343	2.8
Fe II λ2374,2382	3.5
Fe II λ2586	1.6
Fe II λ2599	1.8
Mg II λ2796,2803	3.9

tion features in H1821+643 could investigate the properties of the interstellar medium at large galactocentric distances. We measured the absorption lines listed in Table 5 and indicated by tick marks in Figure 2. The lines are from low-ionization species, except for C IV for which only an upper limit is obtained due to its location on the blue wing of Lyman-α. The C IV λ1548, 1551 absorption is thought to arise in the Galactic halo (Savage 1988). We did not detect any absorption lines in the optical spectrum. An extensive compilation of EWs of absorption lines arising at higher Galactic latitude ($b \sim 60°$, Savage 1988) gives lower values than ours (typically by a factor of about 2) for the low-ionization species except S II, Si II and Al II. Other studies of absorption features arising at lower latitudes [$(l, b) = (96°, 12°)$, Pettini et al. 1982] show the same strong absorption in Mg II λ2796,2803 and Fe II λ2599 as we measured in H1821+643.

In H1821+643, the spectral region between Lyman-α and C IV λ1549 covers the redshift range 0.04–0.27 for detection of C IV absorption lines arising between the QSO and our Galaxy. In this sensitive part of the SWP camera no such absorption features were found above the detection threshold of EW ~ 0.3 Å. The spectral region shortward of the Lyman α emission line allows the detection of low-redshift Lyman α forest lines. Although in the co-added SWP spectrum there are several possible absorption features in this region (e.g., at $\lambda \sim 1470$ and 1490 Å), none were present persistently in all four SWP spectra. The absence of intergalactic Lyman-α and C IV lines is expected for the low redshift of H1821+643 (Bergeron 1988).

4. ACCRETION DISK MODELS

Through studies of variability at different wavelengths (Cutri et al. 1985), and continuum energy distributions between IR, optical, UV, and X-rays (Malkan & Sargent 1982), it has been established that the optical/UV bump is a separate feature from the underlying power law and is now usually attributed to an accretion disk.

In the original model of Shakura & Sunyaev (1973), a summation of Planckian emission arises from the geometrically thin (but optically thick) accretion disk. At the high-frequency side a turnover occurs, corresponding to that blackbody curve with the maximal temperature at the inner disk. There are two free parameters in this model (in addition to the inclination i, and the outer radius of the disk, which affects the low-energy side): the mass M of the central black hole and the accretion rate $\dot{M}$. In addition, the optical continuum generally deviates from the overall power law around 3000 Å. This emission is attributed to Balmer continuum and blended Fe II line emission (Wills, Netzer, & Wills 1985).

Several modifications to the original model have been suggested: inclusion of opacity (e.g., electron scattering and Comptonization) and inclination effects (Czerny & Elvis 1987; Wandel & Petrosian 1988). The Comptonization hardens the emitted spectrum without increasing the energy requirements, and therefore keeps the luminosity sub-Eddington. One of the inclination effects is relativistic focussing of the innermost rays along the disk (Cunningham 1975), resulting in harder spectra for disks which are viewed edge-on. The effects of scattering around the disk have been modeled using stellar atmospheres (Sun & Malkan 1987), resulting in a strong Lyman limit absorption edge for disks observed face-on. However, these authors indicate that blackbody disk models fit the observations better than the models using stellar atmospheres (Sun & Malkan 1989a).

Although alternatives to the thin accretion disk models are available (e.g., the thick torus model by Madau 1988), thin disks are widely used as these have been shown to fit observations of QSOs and Seyfert 1 galaxies successfully (Malkan & Sargent 1982). We calculated disk models for a nonrotating black hole ($a/M = 0$, the Newtonian case), with the standard assumption that the emerging radiation can be described locally by a blackbody spectrum. The temperature T at radius R is given by

$$T(R) = \left\{\frac{3GM\dot{M}}{8\pi\sigma R^3}\left[1 - \left(\frac{R_{in}}{R}\right)^{1/2}\right]\right\}^{1/4}, \quad (1)$$

where R_{in} is the innermost stable orbit ($R_{in} = 3R_{Sch}$, Shakura & Sunyaev 1973). We did not include relativistic effects, since the disk around a nonrotating black hole does not reach close to the black hole (unlike the case of the rotating black hole, where the disk reaches much closer) and the relativistic contributions are, therefore, relatively small. The emergent flux is calculated after fixing the inclination angle such that $\cos i = 0.5$ and assuming a distance D given by

$$D = \frac{cz}{H_0}\left(1 + \frac{z}{2}\right), \quad (2)$$

for $q_0 = 0$ and $H_0 = 50$ km s^{-1} Mpc^{-1}. We did not include a fitting component to account for the Balmer continuum and blended Fe II line emission, and, therefore, our fits deviate from the observed data points between $\log \nu_0 \sim 14.8$ and $\log \nu_0 \sim 15.2$.

The best-fit (by eye) to the 1987 *IUE* data, as shown in Figure 6, with a thin accretion disk model added to the power law, is satisfactory to explain the optical/UV spectrum with the following fitting parameters: $M = (3 \pm 0.5) \times 10^9\ M_\odot$, $\dot{M} = 19 \pm 3\ M_\odot\ \mathrm{yr}^{-1}$, $R_{out}/R_{in} = 12(+5, -3)$, $(L/L_{Edd} = 0.16)$. The fit is constrained at both the high-energy side because of the turnover of the high-frequency *IUE* data points and at the low-energy side due to the steep rise of optical data points. The major sources of uncertainty in the fitting parameters are (1) the nonsimultaneity of the optical and UV data points, (2) the contribution of the Balmer continuum and the Fe II lines, and (3) the correction for interstellar reddening. In this model, the mass of the central object determines mainly the frequency of the peak, while the accretion rate determines mostly the normalization. Once these two parameters have been determined by the turnover in the UV and the strength of the optical/UV bump, respectively, the width of the bump is determined by the extent of the disk, i.e., the ratio R_{out}/R_{in}. The lower limit to R_{out}/R_{in} rules out the possibility of a single blackbody fit, which

would result in a far too narrow bump. If the reality of the UV turnover seen around $\log \nu_0 = 15.3$ is doubted, then the bump could peak at higher frequencies, outside the range of *IUE*. In that case, M would be smaller and the bump would be wider requiring a larger disk (possibly increasing R_{out}/R_{in} to about 30). Such a result is within the range of acceptable fits to the 1989 June *IUE* data, as the short-wavelength turnover is not apparent then. To estimate the uncertainty due to the interstellar reddening correction, we found that $E(B-V) = 0.1$ mag (an increase by about 20%), would increase $\dot{M}$ by about 10%, while M and the size of the disk would remain unchanged. The use of a color excess of $E(B-V) = 0.12$ mag or higher would result in a dereddened spectrum without a turnover, again increasing the uncertainty in M and R_{out}/R_{in}. However, such a large color excess would correspond to a hydrogen column density of 5.8×10^{20} cm^{-2}, far above the values measured near H1821+643.

The novel result of this analysis is the relatively small value of R_{out}/R_{in} (9–17). Bechtold et al. (1987) applied a similar fitting model to the spectrum of PG 1211+143 and found a best fit R_{out}/R_{in} of at least 200, considerably larger than we found in H1821+643. It is of interest to note that the unexpectedly small outer radius in H1821+643 could be identified with the maximum or critical radius (R_{crit}) in the so-called two-temperature accretion flow model of Begelman, Sikora, & Rees (1987). These authors studied the ion torus around a central black hole, and in particular, the cooling effects of electron-positron pair production on such a torus. Due to these cooling effects the torus collapses to a geometrically thin, optically thick annulus in the innermost region, defined by $R < R_{crit} \sim 30\ R_{Sch}$. The thermal UV and possibly the soft X-rays would come from this optically thick region, which would in fact have an outer radius remarkably close to our fit value $R_{out} = 36\ R_{Sch}$ ($R_{out}/R_{in} = 12$). In this model, due to the bistability of the annulus, smooth changes in $\dot{M}$ would cause abrupt changes in the flow structure, which in turn would be responsible for spectral variations. In a stable disk, changes in $\dot{M}$ would affect the emergent spectrum only on the viscosity time scale t_{vis} (Bechtold et al. 1987); for an α disk with the parameters inferred for H1821+643 above, t_{vis} is greater than 6000 yr for $\alpha < 1.0$ (Frank, King, & Raine 1985).

A successful fit of both the optical/UV bump and the *HEAO 1* soft X-ray excess is practically impossible to achieve, considering the decline of the *IUE* data points, and the high and fairly constant flux level for the 0.5–2 keV *HEAO 1* observations. If such a fit is forced (ignoring the nonsimultaneity of the UV and X-ray data), highly super-Eddington luminosities ($L \sim 40\ L_{edd}$) would be produced for the Newtonian accretion disk models, violating the thin disk approximation for the inner disk (Bechtold et al. 1987), unless Compton scattering of the UV photons to EUV and soft X-ray energies is incorporated (Czerny & Elvis 1987). While following the optical data points rather closely, such a fit exceeds the observed UV flux by a factor of about 2–3. Moreover, as there is no evidence that the UV emission and the soft X-ray excess are linked in AGNs (Elvis, Wilkes, & McDowell 1989), there is no convincing justification to fit both features in one model fit for H1821+643 at this moment. This QSO would, however, be an excellent candidate to study whether the UV and soft X-ray radiation have the same physical origin, considering the variability and brightness of both the UV and X-ray emission. In Figure 4 the change in the UV continuum over a period of 4 months is shown. This change in shape, where the spectral hardness is correlated with luminosity, is often found in AGNs which are well observed with *IUE* (Edelson, Krolik, & Pike 1990) and is consistent with an expected increase of temperature with accretion rate. The reported minimum doubling time of about 10 days at X-ray energies (Snyder & Wood 1984) could be identified with the dynamical time scale (t_{dyn}) of the inner disk. We define t_{dyn} as $(1+z)\ R_{max}/v_{max}$, where R_{max} is the radius at which the temperature of the disk reaches a maximum ($R_{max} \sim 8GM/c^2$) and $v_{max} = (GM/R_{max})^{1/2}$. Thus, $t_{dyn} = GM(8/c^2)^{3/2}\ (1+z)$ as seen by the observer, or $t_{dyn} \sim 1.7\ (M/10^9\ M_\odot)$ days.

Sun & Malkan (1989a) presented fits of a thin accretion disk model to the spectra of 24 AGNs, not including H1821+643. As the inferred disk parameters are very similar in the Schwarzschild metric (used by Sun & Malkan 1989a) and the Newtonian metric (used here) for $\cos i = 0.5$, we can compare our values obtained for mass and accretion rate with the large sample. With $M = 3 \times 10^9\ M_\odot$, H1821+643 would be one of the most massive AGNs in the sample and the most massive of the AGNs with intermediate redshift ($z = 0.2$–1.0). The inferred accretion rate of $\dot{M} = 19\ M_\odot\ \mathrm{yr}^{-1}$ would be one of the highest for an intermediate redshift QSOs. This was to be expected, considering the large luminosity of H1821+643 and the pronounced optical/UV bump in its spectrum.

There is, however, one significant difference between our model and that of Sun & Malkan (1989a), and that is the use of the outer radius of the accretion disk. Sun & Malkan (1989a) do not specify their outer radius, but it can be assumed to be a large value. In our fitting model the outer radius is a free parameter, resulting typically in low inferred values for successful fits ($R_{out}/R_{in} \sim 12$). A strong UV/optical bump with a small width, as is the case for H1821+643, can only be fitted in a satisfactory manner with a small accretion disk. While the turnover and the height of the UV bump determine the central mass and accretion rate, the extent of the disk is determined by the width of the bump. We maintain that only a limited disk, in which the range of temperatures is small and therefore the emergent spectrum only slightly broader than the single blackbody curve, fits a narrow optical/UV bump, as observed in H1821+643.

5. CONCLUSIONS

We have obtained multiwavelength observations of H1821+643 and have modeled its continuum with an accretion disk in addition to an underlying power law. The continuum follows the power law with $\alpha = 1.16$ most closely in the far-IR and near-IR, deviating strongly at optical and UV frequencies, and possibly at soft X-ray energies. Most of the energy is emitted in the UV, while the variable soft X-ray excess could have a similar luminosity when at maximum. Fits with a geometrically thin, optically thick accretion disk yield a central black hole mass of $3 \times 10^9\ M_\odot$ and an accretion rate of $19\ M_\odot\ \mathrm{yr}^{-1}$, both large values consistent with the luminosity of H1821+643 and the prominence of the optical/UV bump in its continuum spectrum. The accretion disk fits result in a surprisingly small disk size ($R_{out}/R_{in} = 12$). Efforts to constrain the extreme UV spectrum by applying photoionization models, which predict emission line ratios, were indicative of an ionizing spectrum peaking at UV frequencies.

The shape of the UV continuum spectrum was found to vary significantly, but the time scale of the UV variability remains to be determined by periodic observations. An outstanding question for QSOs with both a strong optical/UV bump and a soft

X-ray excess, of which H1821+643 is a prime example, is whether these components have a common origin. Simultaneous observations at UV and soft X-ray frequencies could determine whether both features are present at the same time. If both emissions arise in an accretion disk, then this should be reflected in the continuum energy distribution and the correlated variability of the UV and soft X-ray flux. To fit both the UV bump and the soft X-ray excess as one feature seems problematic in the current accretion disk models (e.g., requiring highly inclined disks around rapidly rotating holes, as shown by Sun & Malkan 1989a, or the inclusion of a strong Comptonized component, as calculated by Czerny & Elvis 1987). H1821+643, with its strong emission in all wavelength bands (except radio), and its variability in the UV and soft X-ray flux, is an outstanding candidate for simultaneous monitoring in the X-ray and the UV band.

We acknowledge the able assistance of the staff at the Goddard *IUE* Regional Data Analysis Facility. We thank Martin Elvis and Saeqa Vrtilek for obtaining the infrared and optical magnitudes, respectively. This research was supported by NASA *IUE* grants NAG 5-1140 and NAG 5-1425 to the Columbia Astrophysics Laboratory. A. V. F. is supported by NASA grant NAG 5-1171, as well as by NSF grants AST-8957063 and AST-9003829. Lick Observatory is partially funded by NSF Core Block grant AST-8614510. This paper is contribution number 432 of the Columbia Astrophysics Laboratory.

REFERENCES

Bechtold, J., Czerny, B., Elvis, M., Fabbiano, G., & Green, R. F. 1987, ApJ, 314, 699
Begelman, M. C., Sikora, M., & Rees, M. J. 1987, ApJ, 313, 689
Bergeron, J. 1988, in QSO Absorption Lines, ed. J. C. Blades, D. Turnshek, & C. A. Norman (Cambridge: Cambridge University Press), p. 127
Bohlin, R. C., Savage, B. D., & Drake, J. F. 1978, ApJ, 224, 132
Cunningham, C. T. 1975, ApJ, 202, 788
Cutri, R. M., Wisniewski, W. Z., Rieke, G. H., & Lebofsky, M. J. 1985, ApJ, 296, 423
Czerny, B., & Elvis, M. 1987, ApJ, 321, 305
Edelson, R. A., Krolik, J. H., & Pike, G. F. 1990, ApJ, 359, 86
Edelson, R. A., & Malkan, M. A. 1986, ApJ, 308, 59
Elvis, M. 1988, in Supermassive Black Holes, ed. M. Kafatos (Cambridge: Cambridge University Press), p. 131
Elvis, M., Wilkes, B. J., & McDowell, J. C. 1989, in Extreme Ultraviolet Astronomy, ed. R. F. Malina & S. Bowyer (New York: Pergamon)
Filippenko, A. V. 1982, ASP, 94, 715
Frank, J., King, A. R., & Raine, D. J. 1985, in Accretion Power in Astrophysics (Cambridge: Cambridge University Press), p. 101
Grauer, A. D., & Bond, H. E. 1984, ApJ, 277, 211
Kii, T., et al. 1991, in ApJ, in press.
Kinney, A. L., Huggins, P. J., Bregman, J. N., & Glassgold, A. E. 1985, ApJ, 291, 128
Kriss, G. A. 1988, ApJ, 324, 809
Krolik, J. H., & Kallman, T. R. 1988, ApJ, 324, 714
Kwan, J., & Krolik, J. H. 1981, ApJ, 250, 478
Madau, P. 1988, ApJ, 327, 116
Malkan, M. A., & Sargent, W. L. W. 1982, ApJ, 254, 22
Marshall, F. E., Boldt, E. A., Holt, S. S., Mushotsky, R. F., Pravdo, S. H., Rothschild, R. E., & Serlemitsos, P. J. 1979, ApJS, 40, 657
Massey, P., Strobel, K., Barnes, J. V., & Anderson, E. 1988, ApJ, 328, 315
Miller, J. S., & Stone, R. P. S. 1987, the CCD Cassegrain Spectrograph at the Shane Reflector (Lick Observatory Technical Report No. 48, Santa Cruz, CA)
Neugebauer, G., Miley, G. K., Soiffer, B. T., & Clegg, P. E. 1986, ApJ, 308, 815
Nugent, J. J., et al. 1983, ApJS, 51, 1
Oke, J. B., & Gunn, J. E. 1983, ApJ, 266, 713
Pettini, M., et al. 1982, MNRAS, 199, 409
Pravdo, S. H., & Marshall, F. E. 1984, ApJ, 281, 570
Reichert, G. A., Polidan, R. S., Wu, C.-C., & Carone, T. E. 1988, ApJ, 325, 671
Savage, B. D. 1988, in QSO Absorption Lines, ed. J. C. Blades, D. Turnshek, & C. A. Norman (Cambridge: Cambridge University Press), p. 195
Scott, H. A., & O'Dell, S. L. 1989, in IAU Symposium 134, Active Galactic Nuclei, ed. D. E. Osterbrock & J. S. Miller (Dordrecht: Reidel), p. 257
Seaton, M. J. 1979, MNRAS, 187, 73P
Shakura, N. I., & Sunyaev, R. A. 1973, A&A, 24, 337
Snyder, W. A., & Wood, K. S. 1984, in X-ray and UV Emission from Active Galactic Nuclei, ed. W. Brinkman & J. Truemper (Garching: Max Planck Institut), p. 114
Stark, A. A., Heiles, C., Bally, J., & Linke, R. 1990, in preparation
Sun, W.-H., & Malkan, M. A. 1987, in Astrophysical Jets and Their Engines, ed. W. Kundt (Dordrecht: Reidel), p. 125
———. 1989a, ApJ, 346, 68
———. 1989b, in IAU Symposium 134, Active Galactic Nuclei, ed. D. E. Osterbrock & J. S. Miller (Dordrecht: Reidel), p. 262
Turner, M. J. L., et al. 1989, in Proceedings of 23d ESLAB Symp. (Noordwijk, The Netherlands: ESA Publ.), p. 769
Wandel, A., & Petrosian, V. 1988, ApJ, 329, L11
Warwick, R. S., Barstow, M. A., & Yaqoob, T. 1989, MNRAS, 238, 917
Wills, B. J., Netzer, H., & Wills, D. 1985, ApJ, 288, 94
Wood, K. S., et al. 1984, ApJS, 56, 507